Direct numerical simulation of the drag-reducing turbulent boundary layer of viscoelastic fluid

Shinji Tamano[a] and Motoyuki Itoh
Graduate School of Engineering, Nagoya Institute of Technology, Gokiso-cho, Showa-ku, Nagoya, Aichi 466-8555, Japan

Kenichi Hoshizaki
Toyota Technical Development Corporation, Imae, Hanamoto-cho, Toyota, Aichi 470-0334, Japan

Kazuhiko Yokota
Graduate School of Engineering, Nagoya Institute of Technology, Gokiso-cho, Showa-ku, Nagoya, Aichi 466-8555, Japan

(Received 12 September 2006; accepted 22 May 2007; published online 20 July 2007)

Direct numerical simulation of a zero-pressure gradient drag-reducing turbulent boundary layer of homogeneous viscoelastic fluids was performed using constitutive equation models such as the Oldroyd-B and Giesekus models. Mean velocity profiles and turbulence statistics at the different streamwise locations were discussed using both inner and outer scaling. The maximum drag reduction ratio for the Oldroyd-B model, which has the higher elongational viscosity, is larger than for the Giesekus model. The distinct difference in turbulence statistics near the wall between the Oldroyd-B model and Newtonian fluid is observed, as reported in the drag-reducing turbulent channel flow, while in the outer region, distributions of turbulence statistics for the Oldroyd-B model with a drag reduction ratio of about 40% are similar to those for Newtonian fluid. The production term for the turbulent boundary layer does not correspond to the amount of drag reduction, which is consistent with the fact that the streamwise turbulence intensity profile is not a direct indication of the drag reduction. The contribution of the advection term to the budget of streamwise Reynolds normal stress, which does not appear for the turbulent channel flow, is not negligible near the wall for the Oldroyd-B model. For the Oldroyd-B model with a maximum drag reduction ratio of 42%, we can see that quasi-streamwise vortices are weakened and become larger in the streamwise direction, compared to Newtonian fluid. On the other hand, quasi-streamwise vortices for the Giesekus model with a maximum drag reduction ratio of 16% are slightly larger than those for Newtonian fluid. These modifications of near-wall coherent structures are explained by the profile of the trace of mean viscoelastic stress and the elastic energy theory presented by Min *et al.* [J. Fluid Mech. **486**, 213 (2003)] for the drag-reducing turbulent channel flow. © *2007 American Institute of Physics*. [DOI: 10.1063/1.2749816]

I. INTRODUCTION

Velocity measurements of a drag-reducing turbulent channel and pipe flows of viscoelastic fluids have yielded valuable knowledge about the suppression of turbulence, the modification of quasi-streamwise vortices and low-speed streak structures, and the stress defect in which the sum of viscous and turbulent shear stresses is not equal to the total shear stress.[1–15] On the other hand, there have been few experimental studies on the drag-reducing effect of viscoelastic fluids for a turbulent boundary layer, which is a typical external flow.[16–20] Recently, White *et al.*[18] and Hou *et al.*[19] have clarified the effects of polymer additives on the turbulent boundary layer, and Itoh *et al.*[20] found a difference in turbulence statistics between drag-reducing polymer and surfactant fluids for the turbulent boundary layer. These experimental studies have revealed the streamwise variation of turbulence statistics and structures for the turbulent boundary layer of viscoelastic fluids. However, the detailed mechanism of the drag reduction for the turbulent boundary layer flow in which the turbulent and the potential flows are mixed could not be explained by the previous knowledge obtained for the internal flow such as the channel and pipe flows, and has not been well understood.

In the past decade, with the rapid growth of computational resources, direct numerical simulation (DNS) has been performed to investigate the drag-reducing viscoelastic turbulent flows. There have been many DNS studies of turbulent channel flow using constitutive equation models such as the finitely extensible nonlinear elastic-Peterlin (FENE-P) model,[21–34] the Oldroyd-B model,[30,35–37] and the Giesekus model.[22,30,38–41] These numerical investigations have revealed the higher-order turbulence statistics, budgets of kinetic energy and Reynolds stresses, and viscoelastic stress fields (especially elongational stress fields) in which it is considerably difficult or even impossible to obtain them using the experimental measurements. So far, the DNS of drag-reducing turbulent channel flow has become a helpful and

[a]Present address. Telephone: +81 52 735 5609. Fax: +81 52 735 5247. Electronic mail: tamano.shinji@nitech.ac.jp

essential tool for understanding the drag-reducing mechanism of viscoelastic fluids. On the other hand, there are few DNSs of drag-reducing turbulent boundary layer flow of viscoelastic fluids, as far as we know. Quite recently, Dimitropoulos *et al.*[42] performed a DNS of a polymer-induced drag-reducing zero-pressure gradient turbulent boundary layer flow of homogeneous polymer solutions using the FENE-P model. Drag reduction in turbulent boundary layer flow of inhomogeneous polymer solutions was also investigated by Shin and Shaqfeh[43] and Dimitropoulos *et al.*[44] However, it is quite insufficient compared to the DNS of drag-reducing turbulent channel flow.

In the present study, DNSs of a zero-pressure gradient turbulent boundary layer of a drag-reducing homogeneous viscoelastic fluid are performed using constitutive equation models such as the Oldroyd-B and Giesekus models, in which the rheological properties are different. The boundary layer parameters, mean velocity profiles, turbulence statistics, budgets of turbulent energy and Reynolds normal stresses, and near-wall coherent structures such as low-speed streaks and quasi-streamwise vortices are investigated and are compared with those of Newtonian fluid.

II. NUMERICAL METHOD

The nondimensional governing equations for the incompressible viscoelastic flow are continuity and momentum equations,

$$\frac{\partial u_i}{\partial x_i} = 0, \tag{1}$$

$$\frac{\partial u_i}{\partial t} + \frac{\partial (u_i u_j)}{\partial x_j} = -\frac{\partial p}{\partial x_i} + \frac{1-\beta}{\mathrm{Re}_{\theta_0}} \frac{\partial E_{ij}}{\partial x_j} + \frac{\beta}{\mathrm{Re}_{\theta_0}} \frac{\partial^2 u_i}{\partial x_j \partial x_j}, \tag{2}$$

where u_i is the velocity component, p is pressure, x_i is a spatial coordinate, t is time, and E_{ij} is the viscoelastic stress component. In this paper, x_1 (x), x_2 (y), and x_3 (z) directions are streamwise, wall-normal, and spanwise, respectively. $\beta = \eta_s / \eta_0$ is the ratio of solvent viscosity η_s to zero shear rate solution viscosity η_0. For the Giesekus model,[45] the nondimensional constitutive equation for E_{ij} is as follows:

$$E_{ij} + We\left(\frac{\partial E_{ij}}{\partial t} + u_k \frac{\partial E_{ij}}{\partial x_k} - \frac{\partial u_i}{\partial x_k} E_{jk} - E_{ki} \frac{\partial u_j}{\partial x_k} + \alpha E_{jk} E_{ki} \right) = \frac{\partial u_i}{\partial x_j} + \frac{\partial u_j}{\partial x_i}, \tag{3}$$

where α is the mobility factor. The mobility factor α is from 0 to 1, and the Giesekus model with $\alpha = 0$ corresponds to the Oldroyd-B model.[45]

In this study, the inflow condition for the boundary layer is given by the method proposed by Lund *et al.*,[46] so that the computational domain is divided into the main part and driver part in which the inflow condition for the main part is obtained. In the present study, the nondimensional computational parameters are the momentum-thickness Reynolds number Re_{θ_0} and the Weissenberg number We, and they are defined as follows:

$$\mathrm{Re}_{\theta_0} = \frac{\rho U_e \theta_0}{\eta_0}, \tag{4}$$

$$\mathrm{We} = \frac{\lambda U_e}{\theta_0}, \tag{5}$$

where U_e is the free-stream velocity, θ_0 is the momentum-thickness at the inlet plane of the driver part, η_0 is the zero-shear viscosity of the solution, ρ is density, and λ is the relaxation time.

The second-order accurate finite-difference scheme on a staggered grid is used. The velocity components are discretized on the grid cell edges, whereas the pressure and all the components of viscoelastic stress tensors E_{ij} are defined at the center of each cell. The coupling algorithm of the discrete continuity and momentum equations (1) and (2) is based on the second-order splitting method.[47] The resulting discrete Poisson equation for the pressure is solved using the SOR (successive over-relaxation) method after FFT in the periodic (z) direction. The second-order upwind difference scheme is used for the polymer-stress convection term $u_k \partial E_{ij} / \partial x_k$ in (3). An artificial diffusion $\kappa^* \mathrm{We} \partial^2 E_{ij} / \partial x_j^2$ is added in (3) to prevent the numerical instability, where κ^* is the dimensionless artificial diffusion factor. The semi-implicit time marching algorithm is used where the diffusion term in the wall-normal direction is treated implicitly with the Crank-Nicolson scheme, and the third-order Runge-Kutta scheme is used for all other terms.

III. NUMERICAL CONDITION

The nonslip boundary condition $(u = v = w = 0)$ is applied on the wall. The boundary conditions on the top surface of the computational domain are

$$\frac{\partial u}{\partial y} = 0, \quad v = U_e \frac{d\delta^*}{dx}, \quad \frac{\partial w}{\partial y} = 0, \tag{6}$$

where δ^* is the boundary layer displacement thickness. A convective boundary condition,

$$\frac{\partial u_i}{\partial t} + U_e \frac{\partial u_i}{\partial x} = 0, \tag{7}$$

is used at the outlet plane. The inflow condition is generated using the recycle method of Lund *et al.*[46] In the present study, the velocity field data at the streamwise center of the driver part provide inflow data at the inlet of the main part. The boundary conditions of viscoelastic stress components are given by solving the constitutive equations at the wall with the velocity boundary conditions satisfied, except for the inlet boundary at the main part in which the Newtonian velocity data are imposed directly. The periodic boundary conditions for velocity and viscoelastic stress components are imposed in the spanwise direction. The statistically steady Newtonian velocity data are used as the initial condition for the Oldroyd-B model. Moreover, the statistically steady velocity and viscoelastic stress data for the Oldroyd-B model are used as the initial condition for the Giesekus model.

TABLE I. Numerical and physical conditions.

	Newtonian	Oldroyd-B	Giesekus
Re_{θ_0}	500	500	500
We	—	25	25
N_x	256	256	256
N_y	64	64	64
N_z	64	64	64
L_x	$200\theta_0$	$200\theta_0$	$200\theta_0$
L_y	$30\theta_0$	$30\theta_0$	$30\theta_0$
L_z	$20\pi\theta_0/3$	$20\pi\theta_0/3$	$20\pi\theta_0/3$
Δx^+	20	20	20
$\Delta y^+_{\min}-\Delta y^+_{\max}$	0.38–36	0.38–36	0.37–36
Δz^+	8.5	8.4	8.3
α	—	0	0.01
β	1.0	0.9	0.9
$\Delta t U_e/\theta_0$	0.02	0.008	0.008

In the present study, the momentum-thickness Reynolds number Re_{θ_0} is 500 and the Weissenberg number We is 25. The size of the computational domain for the present simulations is equal to $(L_x\times L_y\times L_z)=(200\theta_0\times 30\theta_0\times 20\pi\theta_0/3)$ in the streamwise, wall-normal, and spanwise directions, respectively. The grid size is $(N_x\times N_y\times N_z)=(256\times 64\times 64)$. The grid spacing in x_1 and x_3 directions is uniform, and the wall-normal grids are given by a hyperbolic tangent stretching function. The grid resolution is evaluated by $\Delta x_i^+=\Delta x_i u_\tau/\nu_0$ $(i=1,2,3)$, where Δx_i is the grid spacing in the x_i direction, u_τ is the friction velocity, and $\nu_0=\eta_0/\rho$ is the zero-shear kinematic viscosity of the solution. The mesh spacing in wall units $(\Delta x^+\times\Delta y^+\times\Delta z^+)$ is shown in Table I. It is shown that the present spatial resolution is comparable with that of previous DNS attempts[42] for the corresponding drag-reducing turbulent boundary layer with the same spatial discretization method. We confirmed that for the Newtonian flow, the present numerical results are almost the same as for the grid size of $384\times 64\times 96$. In the driver part, the computational domain and grid size are $(100\theta_0\times 30\theta_0\times 20\pi\theta_0/3)$ and $(128\times 64\times 64)$, respectively, so the grid resolution is almost the same as that of the main part. In the present study, the viscosity ratio β is fixed at 0.9 for the turbulent boundary layer of dilute viscoelastic fluids.[42] The mobility factor α for the Giesekus model is 0.01. Here, the mobility factor α is related to the extensibility of the polymer chains, i.e., the smaller mobility factor corresponds to the larger elongational viscosity. Generally, the Giesekus model represents the shear-thinning property and the moderate elongational viscosity, while the Oldroyd-B model represents the constant shear viscosity and the higher elongational viscosity.[45] The present turbulence statistics are obtained by averaging over space (spanwise direction) and time of over $1000\theta_0/U_e$ after the turbulent flow becomes stationary, where the time increment $\Delta t U_e/\theta_0$ is 0.008 for the Oldroyd-B and Giesekus models and 0.02 for Newtonian fluid, where the time increment for viscoelastic fluid is smaller than half that for Newtonian fluid.[26] In this paper, $^-$ and $'$ represent the time-space (spanwise direction) average and the deviation, respectively. The superscript $^+$ represents the variables normalized by wall variables. The dimensionless artificial diffusion factor κ^* is set to be 0.01.[21] We found that the drag reduction ratio was slightly underestimated due to the addition of the artificial diffusivity, which did not significantly alter turbulence statistics (not shown here).[26,48]

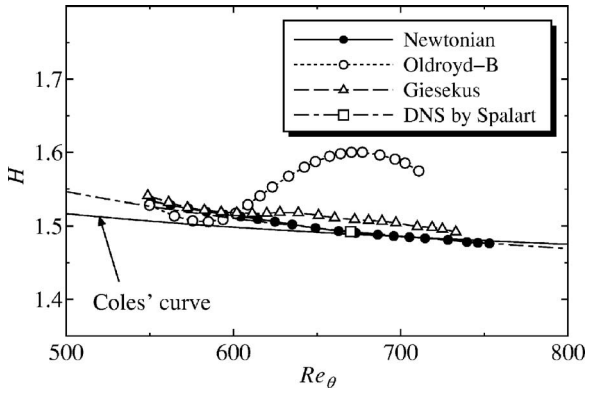

FIG. 1. Shape factor vs Reynolds number.

The validity of the Newtonian code of the turbulent boundary layer is confirmed by comparing our results with the DNS data of Spalart[49] at $\mathrm{Re}_\theta=670$. In addition, the code verification for the drag-reducing flow is also done in the turbulent channel flow at the friction Reynolds number of 150 and the friction Weissenberg number of 30 (see Yu and Kawaguchi[39]).

IV. RESULTS AND DISCUSSION

A. Boundary layer parameters

Figure 1 shows the dependence of the shape factor $H=\delta^*/\delta$ on the momentum-thickness Reynolds number Re_θ. In the figure, the dot-dashed line represents the DNS data of Spalart[49] and the solid line represents Coles' curve[50] for the Newtonian fluid. The data of H for Newtonian fluid agree well with data of Spalart. Near the inlet region $(550\leqslant\mathrm{Re}_\theta\leqslant 600)$, the value of H for the Oldroyd-B model is smaller than that for Newtonian fluid, while for $\mathrm{Re}_\theta>600$, H for the Oldroyd-B model drastically increases with the increase of Re_θ and reaches the maximum at $\mathrm{Re}_\theta\simeq 670$, where H for the Oldroyd-B model is much larger than that for Newtonian fluid and ranges between the value for the laminar flow $(H=2.59)$ and the value for the turbulent flow of Newtonian fluid. On the other hand, H for the Giesekus model agrees well with that for Newtonian fluid in the region $550\leqslant\mathrm{Re}_\theta\leqslant 600$, and is slightly larger for $\mathrm{Re}_\theta>600$.

Figure 2 shows the dependence of the friction coefficient $C_f=2(u_\tau/U_e)^2$ on the momentum-thickness Reynolds number Re_θ. C_f for Newtonian flow is somewhat larger than Coles' curve, possibly due to the effect of grid resolution. The value of C_f for the Oldroyd-B model is larger than that for Newtonian fluid in the region $550\leqslant\mathrm{Re}_\theta\leqslant 600$, and is much smaller for $\mathrm{Re}_\theta>600$. On the other hand, the value of C_f of the Giesekus model is slightly smaller than that for Newtonian fluid in the region $550\leqslant\mathrm{Re}_\theta\leqslant 600$, decreasing with increasing Re_θ in the region $600<\mathrm{Re}_\theta<640$, and is

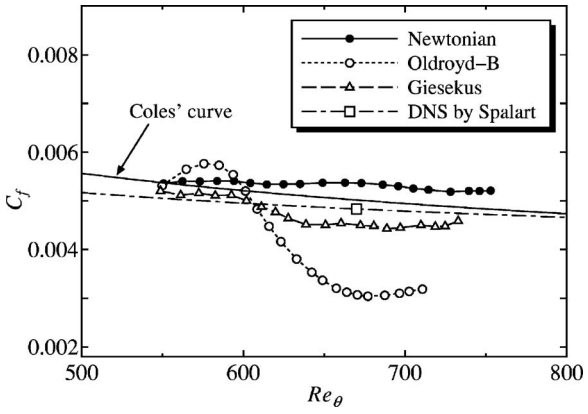

FIG. 2. Friction coefficient vs Reynolds number.

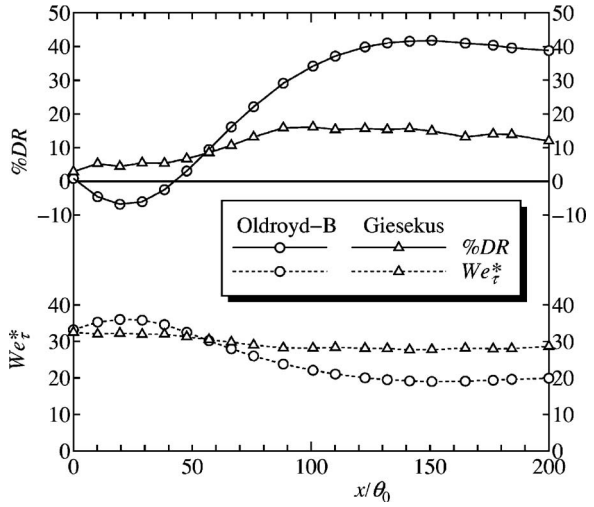

FIG. 3. Streamwise variation of drag reduction ratio and local friction Weissenberg number.

almost constant for $\mathrm{Re}_\theta \geqslant 640$, in which the value for the Giesekus model is much larger than that for the Oldroyd-B model.

B. Drag reduction ratio

The streamwise variation of drag reduction ratio %DR and the local friction Weissenberg number We_τ^* are shown in Fig. 3. %DR is defined as follows:

$$\%\mathrm{DR} = \frac{C_{f,\mathrm{Newtonian}} - C_{f,\mathrm{viscoelastic}}}{C_{f,\mathrm{Newtonian}}} \times 100, \tag{8}$$

at the same streamwise positions. The local friction Weissenberg number We_τ^* is defined as follows:

$$\mathrm{We}_\tau^* = \frac{\lambda u_\tau^2}{\nu_0}. \tag{9}$$

The drag reduction ratio %DR for the Oldroyd-B model is negative and positive in the region $0 < x/\theta_0 < 50$ and for $x/\theta_0 > 50$, respectively. The increase of friction drag (%DR < 0) near the inlet region may be due to the sudden change of velocity fields caused by the unfavorable effect of the inlet boundary condition in which the velocity field data of Newtonian fluid in the driver part is used directly, as pointed out by Dimitropoulos *et al.*[42] Tabor and de Gennes[51] established that turbulence strains are not capable of inducing coil-stretch transition. Polymers are in equilibrium with the mean shear at the inlet and then experience a sudden increase in hydrodynamic forces due to the addition of turbulence. This obviously creates the opportunity for the high extensional viscosity. Naturally, the high extensional viscosity is going to have a dramatic impact on the flow, as reported by Lumley.[52,53] This is because the friction drag increases near the inlet region for the Oldroyd-B model. Note that the same behavior as a function of the streamwise location can also be observed in the drag-reducing turbulent channel flows as a function of time during the initial transient period after the polymer is introduced in the flow (see Min *et al.*[36]). On the other hand, the drag reduction can be seen for the Giesekus model even near the inlet region, and the amount of %DR gradually increases in the streamwise direction. With respect to the transient aspect, Min *et al.*[35–37] observed an overshoot of drag reduction and a relaxation to a steady state for the turbulent channel flow using the Oldroyd-B model. It is noticeable that the duration of the overshoot of drag reduction ratio for the Oldroyd-B model is also observed in this study and it is comparable to the length of the computational domain. Dubief *et al.*[29,32] investigated the correlation between velocity and polymer body force for the turbulent channel flow. For further discussion of the transient aspect, one must investigate the polymer interaction with coherent structures. A parametric study with various mobility factors α and the viscosity ratio β would also be helpful.

The maximum drag reduction ratio (%DR=42) is observed at $x/\theta_0 = 150.8$ for the Oldroyd-B model. The drag reduction ratio for the Giesekus model is maximum (%DR =16) at $x/\theta_0 = 100.8$. It is found that the drag reduction ratio for the Oldroyd-B model is larger than that for the Giesekus model even at the same Weissenberg number (We=25) for the turbulent boundary layer. The same trend has also been reported for the drag-reducing turbulent channel flow.[30] This indicates that high elongational viscosity is important in order to obtain a large drag reduction ratio, and the present result supports the hypotheses suggested by Lumley[52,53] and the early numerical simulation results obtained by Orlandi.[54]

Next, we investigate the relation between the drag reduction ratio %DR and the local friction Weissenberg number We_τ^*. The local friction Weissenberg number We_τ^* represents the ratio of the relaxation time λ and the viscous time ν_0/u_τ^2. Note that Dimitropoulos *et al.*[42,44] and Shin and Shaqfeh[43] used the friction Weissenberg number based on the Newtonian wall shear rate at the inflow plane for the drag-reducing turbulent boundary layer. Lumley[52,53] suggested that drag reduction occurs when the relaxation time is longer than the viscous time. For the Oldroyd-B model, the streamwise location of the minimum of %DR corresponds to that of the maximum of We_τ^*. In addition, the We_τ^* decreases downstream at $30 < x/\theta_0 < 150$, while the drag reduction ratio increases. Note that the amount of %DR increases with the increase of the friction Weissenberg number We_τ for the turbulent channel flow.[35–37] For the Giesekus model, the stream-

TABLE II. Drag reduction ratio.

	Oldroyd-B	Giesekus
$\%DR_{x/\theta_0=19.53}$	−6.79	4.45
$\%DR_{x/\theta_0=100.8}$	34.2	16.1
$\%DR_{x/\theta_0=164.8}$	41.0	13.2

wise variation of We_τ^* is much smaller than that for the Oldroyd-B model. In the present study, the local friction Weissenberg number We_τ^* is rewritten as follows:

$$We_\tau^* = Re_{\theta_0}\left(\frac{u_\tau}{U_e}\right)^2 We. \tag{10}$$

Equation (10) indicates that when the friction velocity u_τ/U_e varies in the streamwise direction owing to the drag-reducing effect, the local friction Weissenberg number We_τ^* also varies for the turbulent boundary layer.

In this study, we obtained turbulence statistics at 20 different streamwise locations. The results at the locations of $x/\theta_0=19.53$ (upstream), $x/\theta_0=100.8$ (center), and $x/\theta_0=164.8$ (downstream) are presented below. The drag reduction ratios at these locations are summarized in Table II for all cases.

C. Mean velocity profiles

Figure 4 shows the profiles of the mean velocity $U^+=U/u_\tau$ in the wall-coordinate $y^+=yu_\tau/\nu$. In the figure, the linear profile $U^+=y^+$, the log-law profile ($U^+=2.44\ln y^+ +5.0$), and Virk's ultimate profile[55] ($U^+=11.7\ln y^+-17$) are presented. The experimental results obtained by White *et al.*[18] and Itoh *et al.*[20] for the drag-reducing turbulent boundary layer of polymer and surfactant solutions, and the experimental data of Itoh *et al.*[20] for the turbulent boundary layer of Newtonian fluid ($Re_\theta=641$), are also shown for comparison. The amount of the drag reduction ratio %DR and the momentum-thickness Reynolds number Re_θ reported in White *et al.*[18] and Itoh *et al.*[20] are (%DR=45, $Re_\theta=1330$) and (%DR=50.1, $Re_\theta=444$), respectively. The present numerical results for the Oldroyd-B model at $x/\theta_0=164.8$, in which the drag reduction ratio is %DR=41.0 and the Reynolds number is $Re_\theta=687$, are compared with these experimental data. It is seen at $x/\theta_0=100.8$ and 164.8 that U^+ for the Giesekus model shifts upward compared to Newtonian fluid, while U^+ for the Oldroyd-B model shifts upward compared to the Giesekus model. This means that the mean velocity shifts upward more as the amount of drag reduction ratio becomes larger, which is consistent with the previous experimental and numerical studies[20,42] of turbulent boundary layers. Min *et al.*[36] also reported that the mean velocity U^+ shifts upward more with the increase of the friction Weissenberg number, i.e., the drag reduction ratio in the DNS of the drag-reducing turbulent channel flow with the Oldroyd-B model. For the Oldroyd-B model, the slope of the velocity profile in the log-law region at $x/\theta_0=164.8$ (%DR=41.0) is steeper than that at $x/\theta_0=100.8$ (%DR=34.2), and approaches those of the experiments[18,20] (see Fig. 4). This corresponds to the fact that the slope of the velocity profile in the large drag reduction ratio regime is larger than that in the small drag reduction regime for the turbulent channel flow.[37] At $x/\theta_0=19.53$, the profile of U^+ in the log-law region shifts slightly up and down for the Giesekus and Oldroyd-B models, respectively. This corresponds to the fact that the drag reduction ratio at $x/\theta_0=19.53$ is positive and negative for the Giesekus and Oldroyd-B models, respectively.

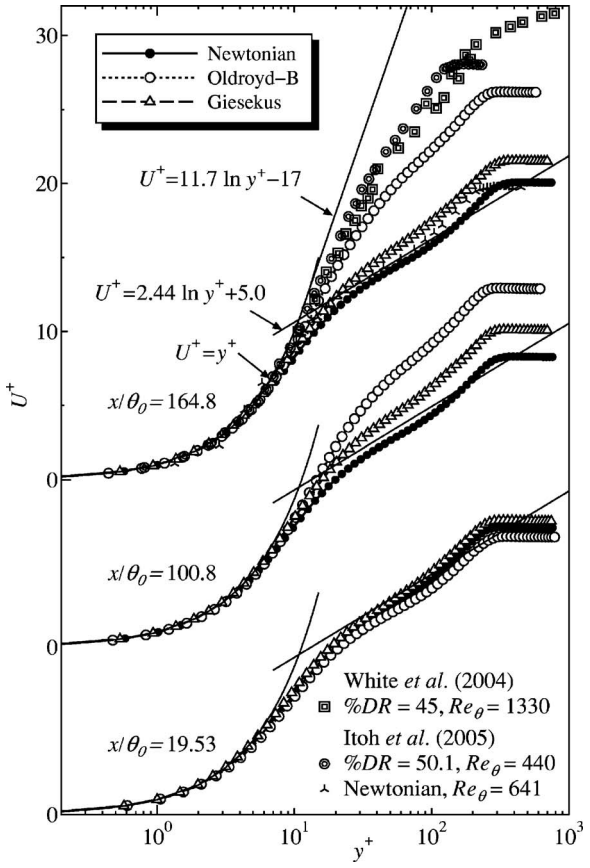

FIG. 4. Mean velocity profiles in wall units.

The distribution of the mean velocity scaled by the free-stream velocity U/U_e is shown in Fig. 5. The abscissa y/δ is the distance from the wall scaled by the boundary layer thickness $\delta=\delta_{99.5}$. At $x/\theta_0=19.53$, the difference in U/U_e

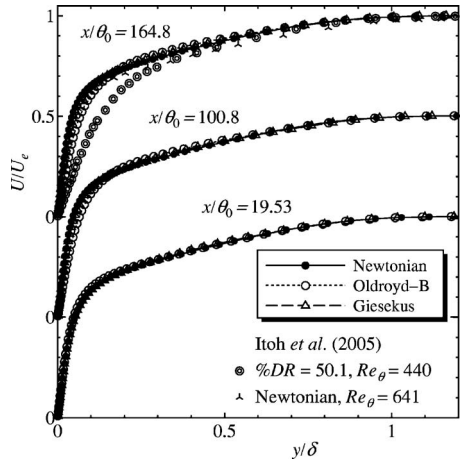

FIG. 5. Mean velocity profiles with outer scaling.

among Newtonian fluid, the Oldroyd-B, and Giesekus models cannot be observed. For the Oldroyd-B model, at $x/\theta_0 = 100.8$ and 164.8, the mean velocity gradient for $y/\delta \leqslant 0.2$ is slightly gentler than that of Newtonian fluid. According to our experimental study[20] for the drag-reducing turbulent boundary layer, the mean velocity scaled by the outer variable is about in the middle between the mean velocity profile for the Newtonian and Blasius laminar profile. Figure 5 obviously shows that the present numerical result of U/U_e is entirely different from that of the experiments.[20] This is because the inlet boundary condition for the present numerical simulation does not correspond to that for the experiment,[20] and the Oldroyd-B and Giesekus models, which are the simple rheological models available, are used.

D. Turbulence statistics

Distributions of the streamwise turbulence intensity scaled by friction velocity $u'^{+}_{\mathrm{rms}} = \overline{u'^2}^{1/2}/u_\tau$ are shown in Fig. 6(a). The maximum streamwise turbulence intensity for the Oldroyd-B model is smaller, slightly larger, and much larger at $x/\theta_0 = 19.53$, 100.8, and 164.8, respectively, compared with the corresponding values for Newtonian fluid. The profile of u'^{+}_{rms} for the Oldroyd-B model at $x/\theta_0 = 164.8$ almost agrees with the experimental data of White *et al.*,[18] although the Reynolds number of the present DNS is much smaller than that of the experiment. Note that the streamwise turbulence intensity of Itoh *et al.*[20] is smaller than that for Newtonian fluid because of the low Reynolds number effect. Min *et al.*[37] found that for the turbulent channel flow, the maximum of streamwise turbulence intensity u'^{+}_{rms} increases with the increase of the drag reduction ratio in the small drag reduction regime, while it decreases in the large drag reduction regime. In the present study for the Oldroyd-B model, the maximum of u'^{+}_{rms} at $x/\theta_0 = 164.8$ is larger than that at $x/\theta_0 = 100.8$ with the smaller drag reduction. However, the maximum value of streamwise turbulence intensity for the turbulent boundary layer is also dependent on the streamwise location, and it is not directly related to the amount of drag reduction, taking account of the result that the maximum of u'^{+}_{rms} for the Oldroyd-B model with %DR=34.2 is comparable with that of Newtonian fluid at $x/\theta_0 = 100.8$. At $x/\theta_0 = 100.8$ and 164.8, the value of y^+ at the maximum of u'^{+}_{rms} for the Oldroyd-B model is larger than that for Newtonian fluid, as reported in previous experimental and numerical studies on drag-reducing turbulent channel flow.[9,10,35–38] This indicates that the buffer layer for the Oldroyd-B model is thicker than that for Newtonian fluid. On the other hand, the streamwise turbulence intensity u'^{+}_{rms} for the Giesekus model with lower drag reduction ratio is slightly larger than that for Newtonian fluid at any streamwise locations. Here, it has been reported that the streamwise turbulence intensity for the Giesekus model is considerably enhanced compared to Newtonian fluid for the drag-reducing turbulent channel flow.[38,40] This difference may be mainly due to the difference in the drag reduction ratio. In order to compare the streamwise turbulence intensity between the Giesekus model and Newtonian fluid, however, we would need to perform the DNS with

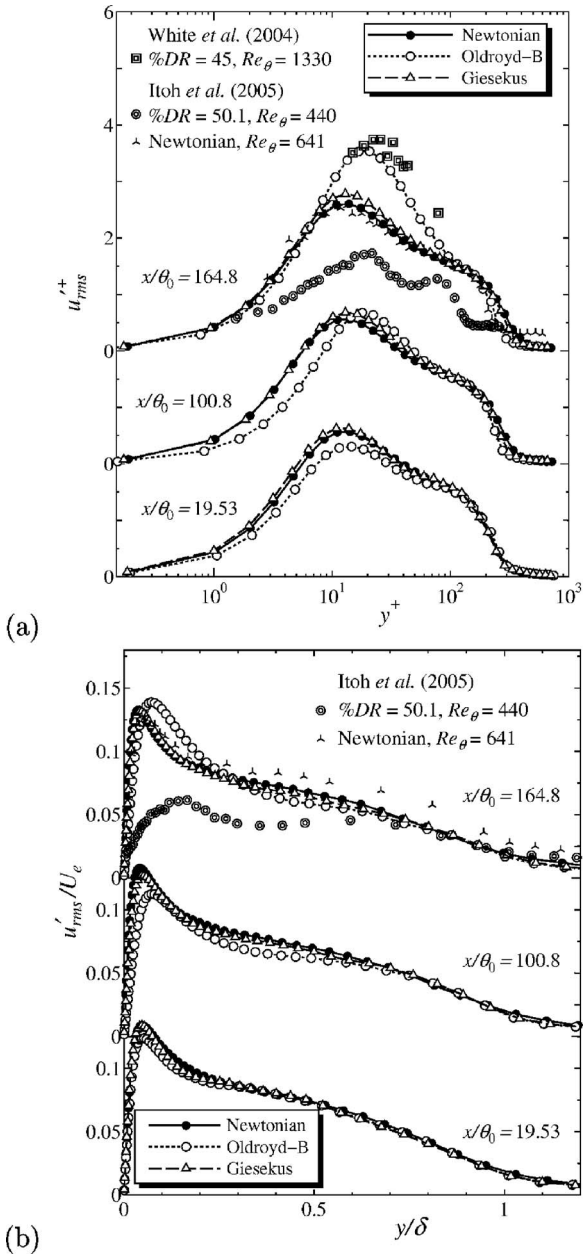

FIG. 6. Profiles of streamwise turbulence intensity: (a) u'^{+}_{rms}, (b) u'_{rms}/U_e.

different mobility factor α and the viscosity ratio β. Readers will be able to refer to our upcoming parametric study in the near future.

Figure 6(b) shows distributions of the streamwise turbulence intensity scaled by free-stream velocity u'_{rms}/U_e. It is found that the profile of u'_{rms}/U_e for the Oldroyd-B model agrees well with that for Newtonian fluid at $y/\delta \geqslant 0.7$, while u'_{rms}/U_e for the Oldroyd-B model does not agree with that for Newtonian fluid at $y/\delta \leqslant 0.2$ as seen in the profile of u'^{+}_{rms}. This is consistent with our experimental measurements[20] in which the profiles of u'_{rms}/U_e are almost the same between the drag-reducing and Newtonian fluids at $y/\delta \geqslant 0.7$ [see Fig. 6(b)]. On the other hand, the discernible difference in u'_{rms}/U_e between the Giesekus model and Newtonian fluid cannot be observed.

Next, distributions of the wall-normal turbulence inten-

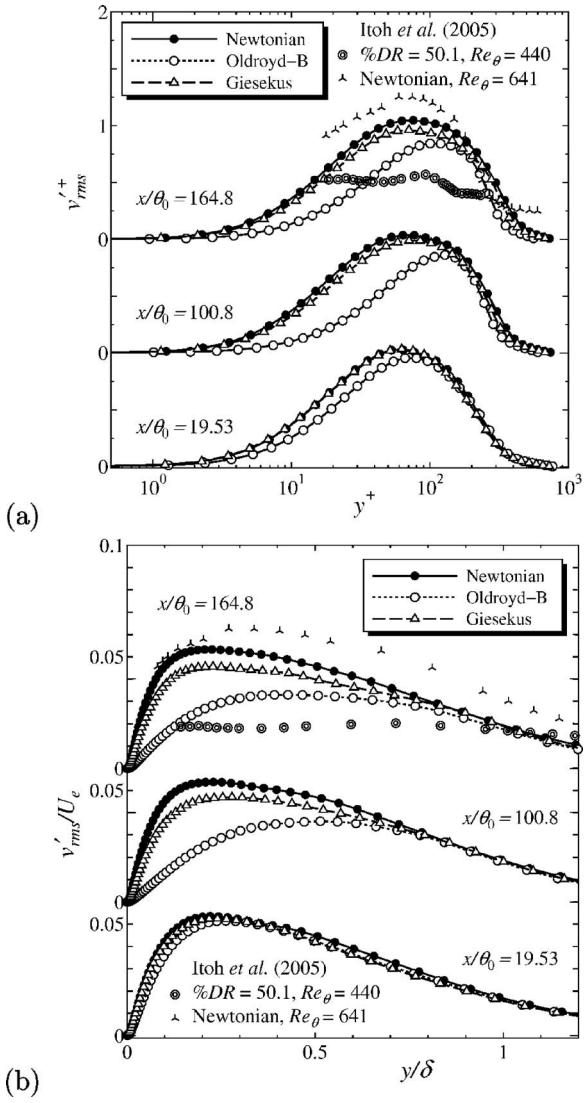

FIG. 7. Profiles of wall-normal turbulence intensity: (a) u'^+_{rms}, (b) u'_{rms}/U_e.

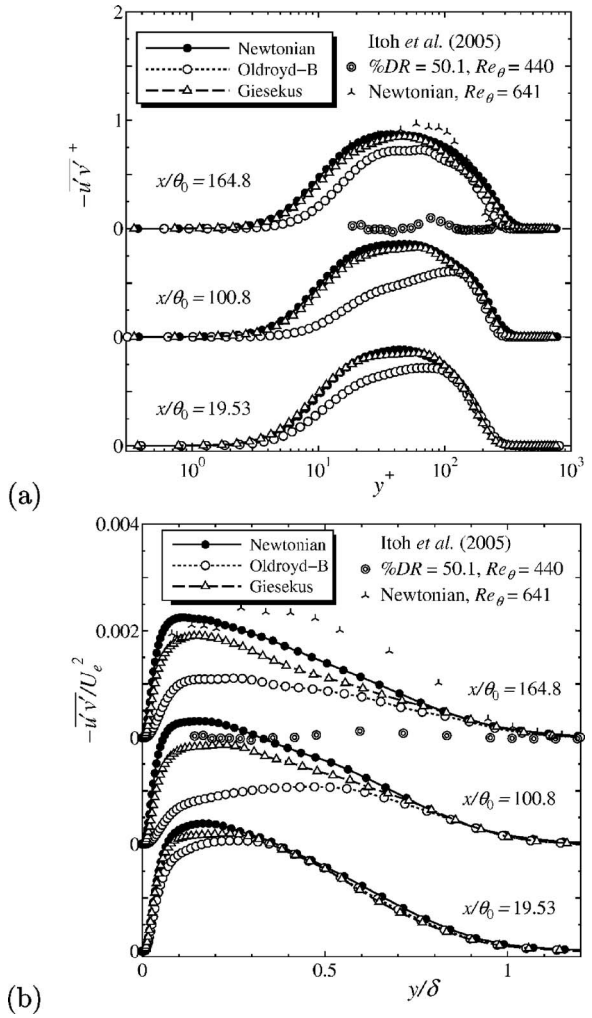

FIG. 8. Profiles of Reynolds shear stress: (a) $-\overline{u'v'}^+$, (b) $-\overline{u'v'}/U_e^2$.

sity v'^+_{rms} are shown in Fig. 7(a). At $x/\theta_0=19.53$, the wall-normal turbulence intensity v'^+_{rms} for the Oldroyd-B model is smaller in the region $5\leqslant y^+\leqslant 100$ than that for Newtonian fluid. At $x/\theta_0=100.8$ and 164.8, the difference in v'^+_{rms} between the Oldroyd-B model and Newtonian fluid is more apparent, which indicates that the velocity fluctuation is considerably attenuated in the wall-normal direction. The similar trend is also reported in the experiments,[20] but the magnitude of the suppression is considerably larger than that of the present simulation and the shape of the profile is largely different, in which v'^+_{rms} for the surfactant solution is almost half that for Newtonian fluid and is virtually constant across the boundary layer. In the drag-reducing turbulent channel flow, the good agreement between the numerical and experimental results has been reported by Min *et al.*[36] using the Oldroyd-B model. The present disagreement may be due to the difference in the inlet boundary condition and the Reynolds number. On the other hand, for the Giesekus model, v'^+_{rms} at $x/\theta_0=19.53$ almost agrees with that of Newtonian fluid, and the maximum of v'^+_{rms} at $x/\theta_0=100.8$ and 164.8 is only slightly smaller than that of Newtonian fluid.

Figure 7(b) shows distributions of the wall-normal turbulence intensity with the outer scaling v'_{rms}/U_e. At $x/\theta_0=19.53$, the difference in v'_{rms}/U_e among Newtonian fluid, the Oldroyd-B model, and the Giesekus model is small. At $x/\theta_0=100.8$, v'_{rms}/U_e for the Oldroyd-B model is much smaller than that for Newtonian fluid near the wall. For the Oldroyd-B model, v'_{rms}/U_e at $x/\theta_0=164.8$ is smaller than that at $x/\theta_0=100.8$, but it is still larger than that of the experiment.[20] Note that v'_{rms}/U_e for the Oldroyd-B model coincides with that for Newtonian fluid at $y/\delta\geqslant 0.7$. It is also noted that the wall-normal turbulence intensity in the drag-reducing turbulent channel flow becomes smaller across the channel. On the other hand, at $x/\theta_0=100.8$ and 164.8, v'_{rms}/U_e for the Giesekus model is smaller than that for Newtonian fluid at $y/\delta\leqslant 0.7$, in which the difference between the Giesekus model and Newtonian fluid is much smaller than that between the Oldroyd-B model and Newtonian fluid. Here, we confirmed that distributions of the spanwise turbulence intensity with the inner and outer scaling were similar to those of the corresponding wall-normal turbulence intensity (not shown here).

Figure 8(a) shows distributions of the Reynolds shear stress scaled by the friction velocity, $-\overline{u'v'}^+=-\overline{u'v'}/u_\tau^2$. The

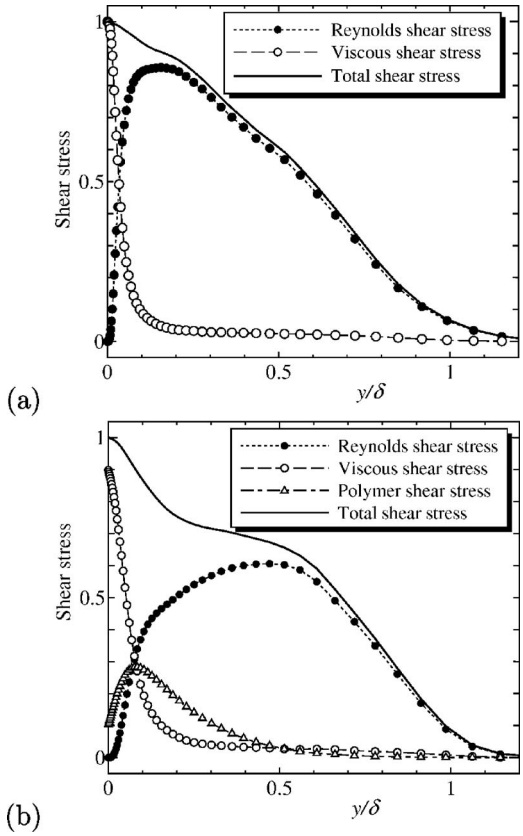

FIG. 9. Profiles of total, Reynolds, viscous, and polymer shear stresses at $x/\theta_0=100.8$: (a) Newtonian fluid, (b) Oldroyd-B model.

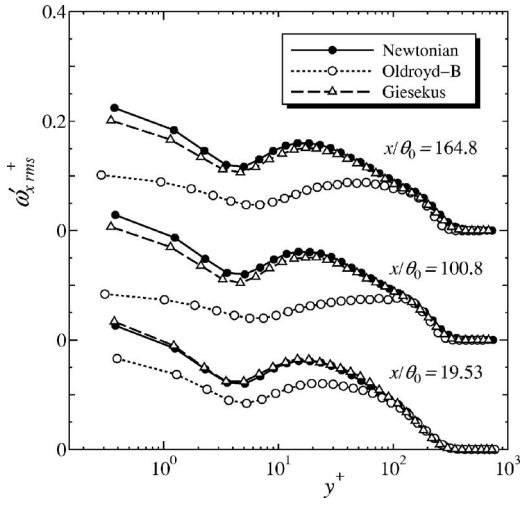

FIG. 10. Profiles of streamwise vorticity fluctuation.

Reynolds shear stress $-\overline{u'v'}^{+}$ for the Oldroyd-B model is smaller in the region $5 \leqslant y^{+} \leqslant 100$ than that for Newtonian fluid at any streamwise locations, and the difference is largest at $x/\theta_0=100.8$. It is known that when the drag reduction ratio is large, the Reynolds shear stress is almost zero in the drag-reducing turbulent flow in viscoelastic fluids.[10,11,13,20] The value of $-\overline{u'v'}^{+}$ for the Oldroyd-B model at $y^{+}>100$ is comparable with that of Newtonian fluid, unlike the DNS result[36] of the turbulent channel flow with the Oldroyd-B model. It is seen that the present numerical result does not predict the experiment[20] where the Reynolds shear stress is almost zero across the boundary layer. Even in the recent studies[26,33,34,37,41] on the DNS of the drag-reducing turbulent channel flow in the large (high) or the maximum drag reduction regimes, the almost zero Reynolds shear stress profile could not be obtained. This indicates that some kinds of improved or even new constitutive equation models would be needed for predicting the experimental results more accurately. On the other hand, no distinct difference in $-\overline{u'v'}^{+}$ would be observed between the Giesekus model and Newtonian fluid.

Figure 8(b) shows distributions of the Reynolds shear stress $-\overline{u'v'}/U_e^{2}$. At $x/\theta_0=100.8$ and 164.8, $-\overline{u'v'}/U_e^{2}$ for the Oldroyd-B model is much smaller than that for Newtonian fluid at $y/\delta \leqslant 0.7$, and is smaller than half at $y/\delta \simeq 0.2$. On the other hand, the difference in $-\overline{u'v'}/U_e^{2}$ between the Giesekus model and Newtonian fluid is smaller than that between the Oldroyd-B model and Newtonian fluid, but the difference with the outer scaling becomes clearer than that with the inner scaling.

Next, we compare the total shear stress profiles between Newtonian fluid and the Oldroyd-B model. The total shear stress T_{12} is defined as follows:

$$T_{12}=-\overline{u'v'}+\frac{1}{\mathrm{Re}_{\theta_0}}\frac{dU}{dy}+\frac{1-\beta}{\mathrm{Re}_{\theta_0}}\frac{d\bar{E}_{12}}{dy}, \tag{11}$$

where $-\overline{u'v'}$ is the Reynolds shear stress, $(dU/dy)/\mathrm{Re}_{\theta_0}$ is the viscous shear stress, and $(1-\beta)(d\bar{E}_{12}/dy)/\mathrm{Re}_{\theta_0}$ is the polymer shear stress. Figure 9 shows that for the Oldroyd-B model, the polymer shear stress is maximum at $y/\delta=0.1$, and occupies about 30% of the total shear stress there. Note that the ordinate is scaled by the inner variables. In addition, the polymer shear stress is almost zero for $y/\delta>0.7$, which corresponds to the fact that the Reynolds shear stress profile agrees well with that for Newtonian fluid at $y/\delta>0.7$ [see Fig. 8(b)].

Figure 10 shows distributions of rms of the streamwise vorticity fluctuation scaled by inner variables. At any streamwise locations, $\omega'^{+}_{x\mathrm{rms}}$ for the Oldroyd-B model is much smaller than that for Newtonian fluid at $y^{+}<100$, while it agrees well with that for Newtonian fluid at $y^{+}>100$. At $x/\theta_0=100.8$ and 164.8, the maximum of $\omega'^{+}_{x\mathrm{rms}}$ for the Oldroyd-B model appears at $y^{+}\simeq 100$, and the wall-normal locations of the maximum move considerably away from the wall compared to the location for Newtonian fluid ($y^{+}\simeq 20$). Note that the location of minimum $\omega'^{+}_{x\mathrm{rms}}$ for the Oldroyd-B model ($y^{+}\simeq 5$) is almost the same as that for Newtonian fluid. Here, it has been reported that the locations of the minimum and maximum of the rms of streamwise vorticity fluctuation correspond to the average locations of lower limits and the center of the quasi-streamwise vortices near the wall, respectively.[56] Therefore, it can be deduced that the quasi-streamwise vortices become larger away from the wall, compared to Newtonian fluid. The same trend has also been reported in the drag-reducing turbulent channel flows,[22,36] but the amount of the shift in the wall-normal direction ob-

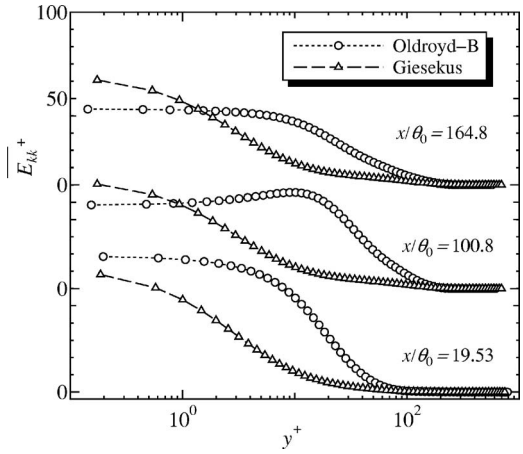

FIG. 11. Trace of mean viscoelastic stress.

served in the present study is much larger. On the other hand, the profile of $\omega'^+_{x\mathrm{rms}}$ for the Giesekus model virtually agrees with that for Newtonian fluid at any streamwise locations.

Figure 11 shows distributions of the trace of mean viscoelastic stress $\overline{E_{kk}}^+$, which represents the magnitude of the polymer elongation. At any streamwise locations, $\overline{E_{kk}}^+$ for the Oldroyd-B model is larger than that for the Giesekus model in the region $1 \leqslant y^+ \leqslant 50$. For the Oldroyd-B model, the value of $\overline{E_{kk}}^+$ in the region $1 \leqslant y^+ \leqslant 50$ at $x/\theta_0 = 100.8$ is larger than that at $x/\theta_0 = 164.8$. Here, the increasing rate of the drag reduction ratio %DR in the streamwise direction is relatively large near the center of the computational domain $(x/\theta_0 = 100.8)$, and the %DR slightly decreases near the downstream of the computational domain $(x/\theta_0 = 164.8)$ (see Fig. 3). From these results, it can be deduced that turbulence statistics are strongly affected in the buffer layer by the high elongational viscosity, and the effect appears significantly in the region of center to downstream. Note that in the region very close to the wall $(y^+ < 1)$, $\overline{E_{kk}}^+$ for the Giesekus model is larger than that for the Oldroyd-B model at $x/\theta_0 = 100.8$ and 164.8.

E. Budgets of turbulent kinetic energy

The budget data obtained by DNS are very helpful for understanding the modification of turbulence statistics and the drag-reducing mechanism. Therefore, budgets of turbulent kinetic energy have been investigated for the drag-reducing turbulent channel flow.[23,25,26,35–37,40] But budgets of turbulent kinetic energy remain unclear for the drag-reducing turbulent boundary layer. The equation for the turbulent kinetic energy $k = \overline{u'_i u'_i}/2$ is as follows in the drag-reducing turbulent boundary layer:

$$-A_k + T_k^{(\Pi)} + T_k^{(\nu)} + \varepsilon_k + T_k^{(t)} + P_k + T_k^{(p)} + W_k = 0, \tag{12}$$

where advection term A_k, pressure diffusion term $T_k^{(\Pi)}$, viscous diffusion term $T_k^{(\nu)}$, dissipation term ε_k, turbulent diffusion term $T_k^{(t)}$, production term P_k, polymer diffusion term $T_k^{(p)}$, and polymer stress work term W_k are defined as

$$A_k = U_j \frac{\partial}{\partial x_j}\left(\frac{1}{2}\overline{u'_i u'_i}\right), \tag{13}$$

$$T_k^{(\Pi)} = -\frac{\partial}{\partial x_i}(\overline{u'_i p'}), \tag{14}$$

$$T_k^{(\nu)} = \frac{\beta}{\mathrm{Re}}\frac{\partial^2}{\partial x_j \partial x_j}\left(\frac{1}{2}\overline{u'_i u'_i}\right), \tag{15}$$

$$\varepsilon_k = -\frac{\beta}{\mathrm{Re}}\overline{\frac{\partial u'_i}{\partial x_j}\frac{\partial u'_i}{\partial x_j}}, \tag{16}$$

$$T_k^{(t)} = -\frac{\partial}{\partial x_j}\left(\frac{1}{2}\overline{u'_i u'_i u'_j}\right), \tag{17}$$

$$P_k = -\overline{u'_i u'_j}\frac{\partial U_i}{\partial x_j}, \tag{18}$$

$$T_k^{(p)} = \frac{1-\beta}{\mathrm{Re}}\frac{\partial}{\partial x_j}(\overline{u'_i E'_{ij}}), \tag{19}$$

$$W_k = -\frac{1-\beta}{\mathrm{Re}}\overline{E'_{ij}\frac{\partial u'_i}{\partial x_j}}. \tag{20}$$

In the above equations, the contribution of the viscoelastic stress to the turbulent kinetic energy equation appears through the polymer diffusion term $T_k^{(p)}$ and the polymer stress work term W_k.

Figure 12 shows the budget of turbulent kinetic energy k^+ at $x/\theta_0 = 100.8$, in which the abscissa and ordinate are scaled by the inner variables and the symbols are plotted at the three points. The magnitudes of the production term P_k and the dissipation term ε_k, which are dominant terms for the Oldroyd-B model, are much smaller than those for Newtonian fluid. The same trend for the Oldroyd-B model has been reported for the drag-reducing turbulent channel flow.[36,37] On the other hand, the magnitudes of P_k and ε_k for the Giesekus model are slightly smaller than those for Newtonian fluid. For the Oldroyd-B model, the polymer stress work term W_k is comparable with the dissipation term ε_k for $y^+ > 50$. For the Giesekus model, the contribution of W_k to the turbulent kinetic energy budget is smaller than that for the Oldroyd-B model. However, the distinct difference in the budget of k^+ between the Giesekus model and Newtonian fluid has been reported for the drag-reducing turbulent channel flow.[40] This difference may be mainly due to the difference in the drag reduction ratio. The polymer diffusion term $T_k^{(p)}$ is negligible for both the Oldroyd-B and Giesekus models.

Figure 13 shows the distributions of the production term P_k at $x/\theta_0 = 19.53$, 100.8, and 164.8. For the Oldroyd-B model, the production term P_k at $x/\theta_0 = 100.8$ is smaller than those at $x/\theta_0 = 19.53$ and 164.8. Min *et al.*[36] reported that the production and dissipation of the turbulent kinetic energy for the Oldroyd-B model decrease throughout the channel with the drag reduction ratio (the friction Weissenberg number). It is noticeable that the production term P_k at $x/\theta_0 = 100.8$ with %DR = 34.2 is smaller than P_k at $x/\theta_0 = 164.8$ with %DR = 41.0 in this study. This indicates that the production term for the turbulent boundary layer does not correspond to the amount of the drag reduction, which is consistent with the

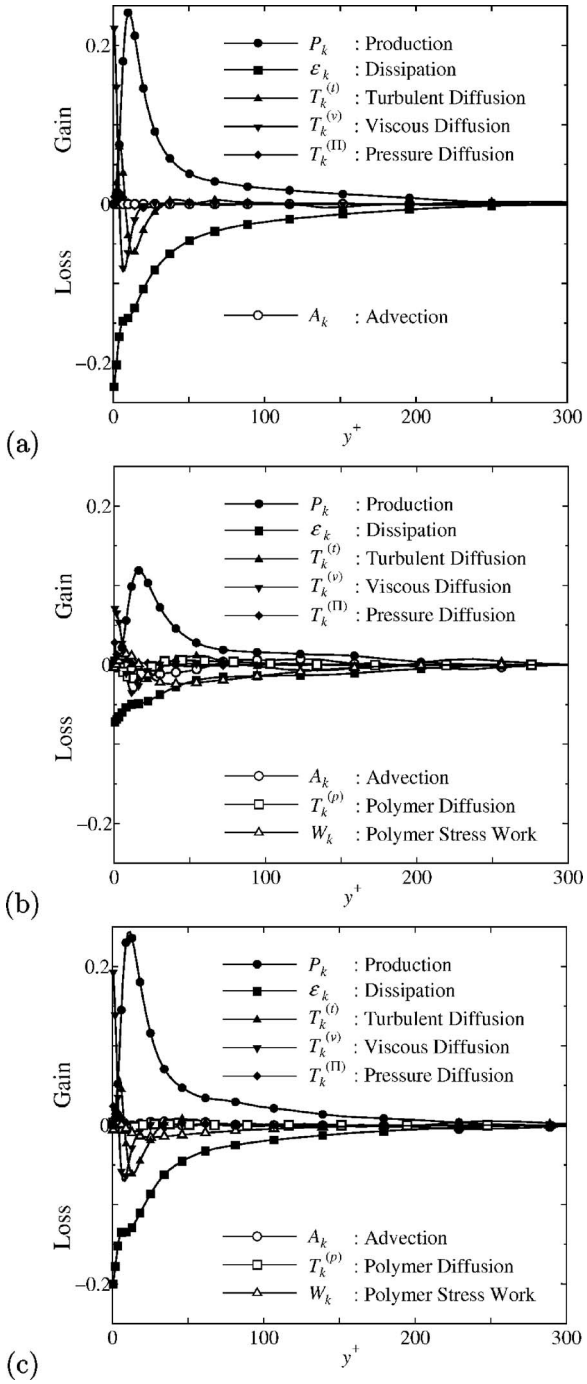

FIG. 12. Budgets of turbulent kinetic energy k^+ at $x/\theta_0=100.8$: (a) Newtonian fluid, (b) Oldroyd-B model, and (c) Giesekus model.

fact that the streamwise turbulent intensity profile is not a direct indication of the drag reduction (see Fig. 6). At $x/\theta_0=100.8$ and 164.8, the maximum locations of P_k for the Oldroyd-B model move away from the wall, compared with those for Newtonian fluid. This corresponds to the fact that the maximum location of streamwise turbulence intensity moves away from the wall (see Fig. 6). On the other hand, the profiles of P_k for the Giesekus model are close to those for Newtonian fluid at any streamwise locations. In the DNS data[40] on the drag-reducing turbulent channel flow with the higher drag reduction for the Giesekus model, the decrease in

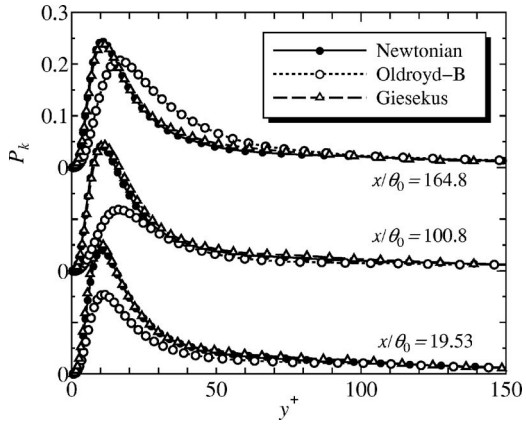

FIG. 13. Distributions of production terms.

the magnitude of the production term is considerably large. For both the Oldroyd-B and Giesekus models, the viscoelastic effect on the production term is negligible for $y^+>100$.

Figure 14 shows distributions of the polymer stress work term W_k. For the Oldroyd-B model, W_k at $x/\theta_0=100.8$ attains its maximum at $y^+\simeq 10$ and is larger than those at $x/\theta_0=19.53$ and 164.8. In addition, W_k for the Oldroyd-B model at $x/\theta_0=19.53$ has the negative peak at $y^+\simeq 20$, and the location of the negative peak shifts away from the wall ($y^+\simeq 30$) at $x/\theta_0=100.8$. As a whole, the polymer stress work term for the Oldroyd-B model makes a negative contribution to the budget, as reported by Ptasinski *et al.*[26] The magnitudes of the maximum and the minimum of W_k for the Giesekus model are smaller than those for the Oldroyd-B model, respectively. It is noted that the contribution of the polymer stress work to the turbulent kinetic energy budget for the Oldroyd-B model with the larger drag reduction ratio is larger, compared to the Giesekus model. This is supported by Ptasinski *et al.*,[26] who showed that the polymer stress work becomes more important with increasing the drag reduction ratio for the turbulent channel flow.

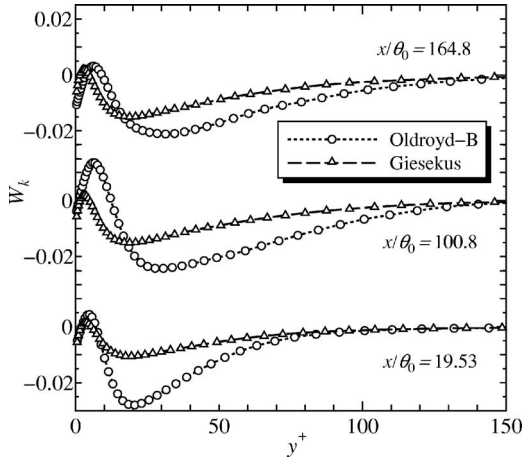

FIG. 14. Distributions of polymer stress work terms.

F. Budgets of Reynolds normal stresses

Budgets of Reynolds normal stresses for the drag-reducing turbulent boundary layer have not been investigated, although there are a few investigations of the drag-reducing turbulent channel flow.[23,24,26,40] The equation for the Reynolds stress $\overline{u_i' u_j'}$ is as follows in the drag-reducing turbulent boundary layer:

$$-A_{ij} + T_{ij}^{(\Pi)} + R_{ij} + T_{ij}^{(\nu)} + \varepsilon_{ij} + T_{ij}^{(t)} + P_{ij} + T_{ij}^{(p)} + W_{ij} = 0, \tag{21}$$

where advection term A_{ij}, pressure diffusion term $T_{ij}^{(\Pi)}$, pressure-strain correlation term R_{ij}, viscous diffusion term $T_{ij}^{(\nu)}$, dissipation term ε_{ij}, turbulent diffusion term $T_{ij}^{(t)}$, production term P_{ij}, polymer diffusion term $T_{ij}^{(p)}$, and polymer stress work term W_{ij} are defined as

$$A_{ij} = U_k \frac{\partial(\overline{u_i' u_j'})}{\partial x_k}, \tag{22}$$

$$T_{ij}^{(\Pi)} = -\frac{\partial}{\partial x_j}(\overline{u_i' p'}) - \frac{\partial}{\partial x_i}(\overline{u_j' p'}), \tag{23}$$

$$R_{ij} = \overline{p' \frac{\partial u_i'}{\partial x_j}} + \overline{p' \frac{\partial u_j'}{\partial x_i}}, \tag{24}$$

$$T_{ij}^{(\nu)} = \frac{\beta}{\mathrm{Re}} \frac{\partial^2}{\partial x_k \partial x_k}(\overline{u_i' u_j'}), \tag{25}$$

$$\varepsilon_{ij} = -2\frac{\beta}{\mathrm{Re}} \overline{\frac{\partial u_i'}{\partial x_k} \frac{\partial u_j'}{\partial x_k}}, \tag{26}$$

$$T_{ij}^{(t)} = -\frac{\partial}{\partial x_k}(\overline{u_i' u_j' u_k'}), \tag{27}$$

$$P_{ij} = -\overline{u_i' u_k'} \frac{\partial U_j}{\partial x_k} - \overline{u_j' u_k'} \frac{\partial U_i}{\partial x_k}, \tag{28}$$

$$T_{ij}^{(p)} = \frac{1-\beta}{\mathrm{Re}} \frac{\partial}{\partial x_k}(\overline{u_i' E_{jk}'} + \overline{u_j' E_{ik}'}), \tag{29}$$

$$W_{ij} = -\frac{1-\beta}{\mathrm{Re}} \left(\overline{E_{jk}' \frac{\partial u_i'}{\partial x_k}} + \overline{E_{ik}' \frac{\partial u_j'}{\partial x_k}} \right). \tag{30}$$

Figure 15 shows budgets of the streamwise Reynolds normal stress $\overline{u'u'}^+$ at $x/\theta_0 = 100.8$ for Newtonian fluid and the Oldroyd-B model, in which the scale of the ordinate is different between Figs. 15(a) and 15(b). The production term P_{11} and the dissipation term ε_{11} for the Oldroyd-B model are much smaller than those for Newtonian fluid. For the Oldroyd-B model, the contribution of the polymer diffusion term $T_{11}^{(p)}$ and the polymer stress work term W_{11} to the budget are comparable with that of the turbulent diffusion term $T_{11}^{(t)}$, and are not negligible. The contribution of A_{11} to the budget is almost zero for Newtonian fluid, but it is not negligible near the wall for the Oldroyd-B model. Note that the contribution of the advection term A_{11} does not appear for the turbulent channel flow. We confirmed that the budget of $\overline{u'u'}^+$ for the Giesekus model was similar to that for Newtonian fluid (not shown here).

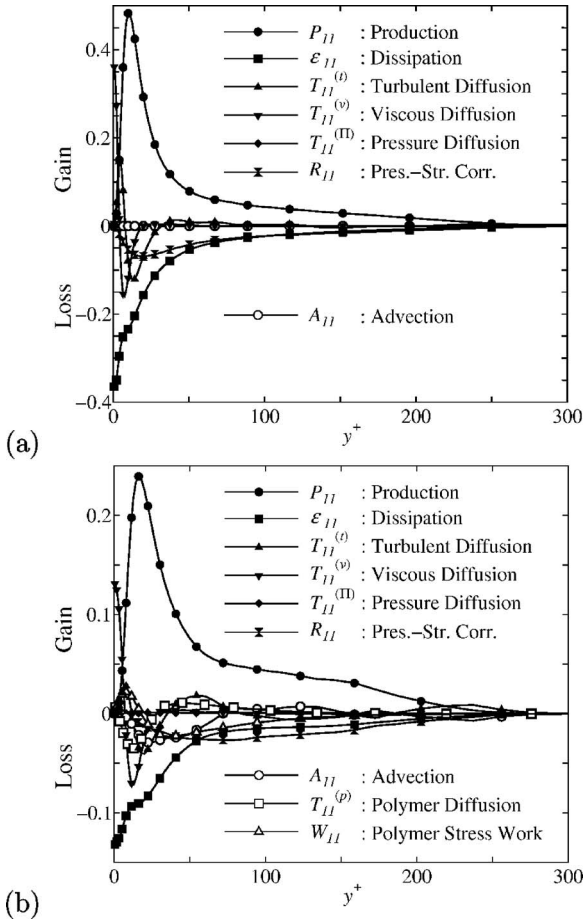

FIG. 15. Budgets of $\overline{u'u'}^+$ at $x/\theta_0 = 100.8$: (a) Newtonian fluid, (b) Oldroyd-B model.

Figure 16 shows budgets of the wall-normal Reynolds normal stress $\overline{v'v'}^+$ at $x/\theta_0 = 100.8$ for Newtonian fluid and the Oldroyd-B model. For Newtonian fluid, the maximum of the pressure-strain correlation term R_{22} and the minimum of the dissipation term ε_{22} definitely appear at $y^+ \simeq 25$, while such a maximum and minimum do not appear for the Oldroyd-B model. For the Oldroyd-B model, in the region $50 < y^+ < 100$, the contribution of the polymer stress work term W_{22} to the budget is larger than that of the dissipation term ε_{22}, and W_{22} is dominant in addition to the pressure-strain correlation term R_{22}. The same trend has been found in the DNS[24,26,40] of the drag-reducing turbulent channel flow with the FENE-P and Giesekus models.

Figure 17 shows profiles of the streamwise, wall-normal, and spanwise pressure-strain correlation terms. For the Oldroyd-B model, R_{11}, R_{22}, and R_{33} for $y^+ \leqslant 100$ are much smaller than those for Newtonian fluid. This implies that the redistribution of turbulent energy from the streamwise velocity components to wall-normal and spanwise velocity components is strongly suppressed for the Oldroyd-B model, as well as the drag-reducing turbulent channel flow.[23,26,40] This result also corresponds to the fact that the streamwise and wall-normal turbulence intensities for the Oldroyd-B model

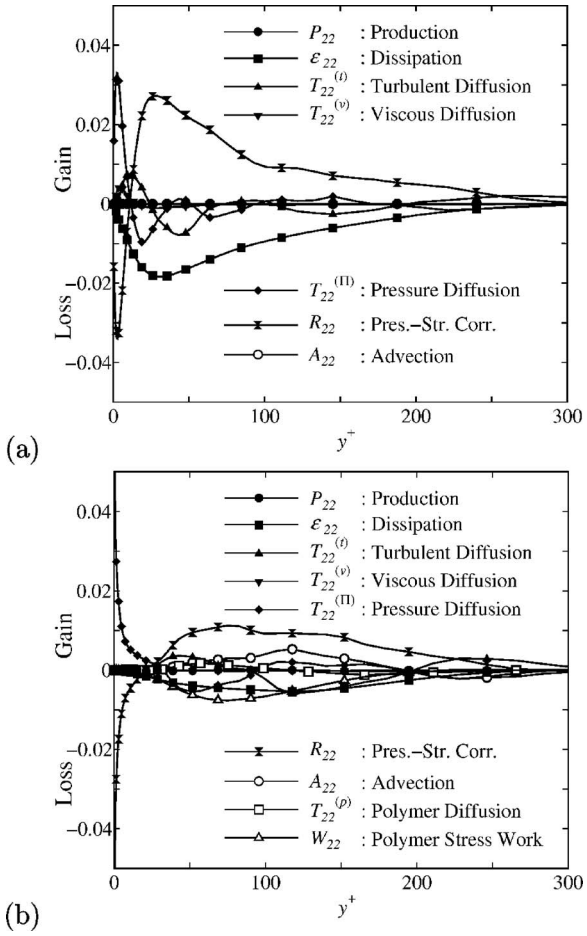

FIG. 16. Budgets of $\overline{v'v'}^+$ at $x/\theta_0=100.8$: (a) Newtonian fluid, (b) Oldroyd-B model.

become larger and smaller, respectively, compared to Newtonian fluid (see Figs. 6 and 7). This has also been pointed out in the drag-reducing turbulent channel flow.[23,24,26,40] Therefore, it can be deduced that the mechanism of the modification of turbulence statistics and coherent structures

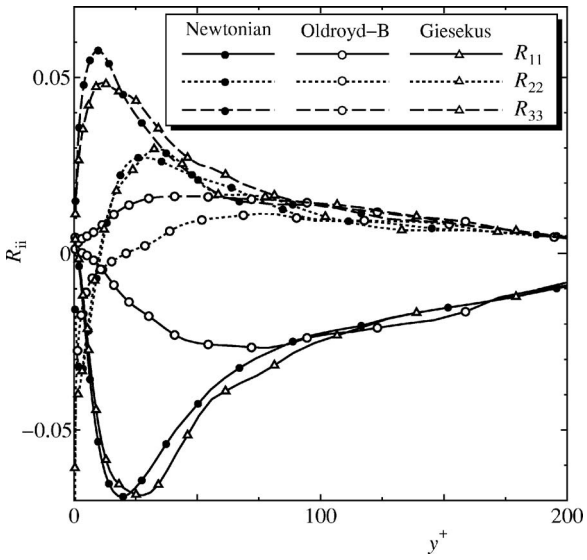

FIG. 17. Distributions of pressure-strain correlation terms at $x/\theta_0=100.8$.

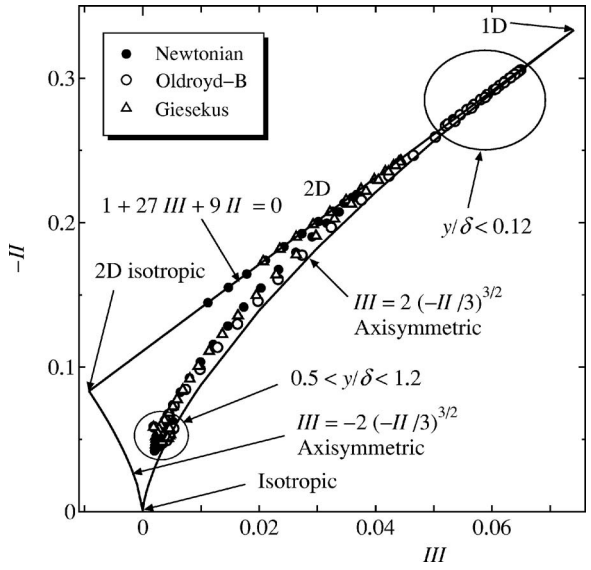

FIG. 18. Anisotropy invariant map for Reynolds stress tensor at $x/\theta_0=100.8$.

near the wall is similar for both the turbulent boundary layer and channel flow. The difference in the pressure-strain correlation terms between the Giesekus model and Newtonian fluid is much smaller than that between the Oldroyd-B model and Newtonian fluid.

Figure 18 shows the anisotropy invariant map[57] for the Reynolds stress tensor at $x/\theta_0=100.8$, where the drag reduction ratios for the Oldroyd-B and Giesekus models are 34.2% and 16.1%, respectively. In the figure, the abscissa and ordinate are the second invariant $II=-b_{ij}b_{ji}/2$ and the third invariant $III=b_{ij}b_{jk}b_{ki}/3$ of the anisotropy tensor $b_{ij}=\overline{u_i'u_j'}/\overline{u_k'u_k'}-\delta_{ij}$, respectively. Compared to the Giesekus model, the Oldroyd-B model shows more anisotropic behavior of the Reynolds stress tensor near the wall ($y/\delta<0.12$), in which the second and third invariants approach the one-dimensional component state. In addition, the near-wall turbulence for the Giesekus model is more anisotropic than that for the Newtonian fluid. This indicates that the near-wall turbulence becomes more anisotropic with increasing the drag reduction ratio.

Dubief *et al.*[32] found that drag reducing flows were dramatically more anisotropic than the Newtonian flow. Jovanović *et al.*[58] and Frohnapfel *et al.*[59] also reported that the anisotropic state of near-wall turbulence is shifted to a higher value as the drag reduction ratio increases. Their findings for the turbulent channel flow support our numerical results for the turbulent boundary layer. The present trend of the anisotropy invariant map supports the fact that the magnitude of the pressure-strain correlation terms near the wall is much smaller than that for Newtonian fluid (see Fig. 17), as mentioned by Dubief *et al.*[32] for the turbulent channel flow. In the region from the center to the edge of the boundary layer ($0.5<y/\delta<1.2$), the invariants of the Reynolds stress tensor for Newtonian fluid and the Oldroyd-B and Giesekus models approach the isotropic state, and no distinct difference is observed among them.

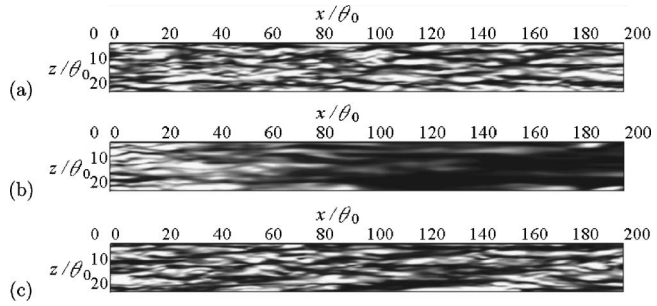

FIG. 19. Contour of streamwise velocity ($0.1 \leqslant u/U_e \leqslant 0.4$, black to white) in the x-z plane at $y/\theta_0=0.152$: (a) Newtonian fluid, (b) Oldroyd-B model, and (c) Giesekus model.

G. Coherent structures

Figure 19 shows the contour of streamwise velocity in the x-z plane at $y/\theta_0=0.152$, which corresponds to $y^+=3-4$ for Newtonian fluid, the Oldroyd-B model, and the Giesekus model, and corresponds to the region within the viscous sublayer. For the Oldroyd-B model, the low-speed region (black) expands in the spanwise direction, and the near-wall streak structures for $x/\theta_0>50$ are considerably larger than that for Newtonian fluid. On the other hand, the near-wall streak structures for the Giesekus model seem to be slightly larger than that for Newtonian fluid.

To compare the spanwise spacing of near-wall streaks among Newtonian fluid and the Oldroyd-B and Giesekus models, the profiles of the two-point correlation coefficients of streamwise velocity fluctuation R_{uu} at $y/\theta_0=0.152$ and $x/\theta_0=100.8$ are shown in Fig. 20. The two-point correlation coefficient R_{uu} is defined as follows:

$$R_{uu}=\frac{\overline{u'(z)u'(z+r_z)}}{\overline{u'^2}}. \tag{31}$$

In the figure, the abscissa $r_z^+=r_z u_\tau/\nu$ is the spanwise separation scaled by wall variables. The first minimum of R_{uu} appears at $r_z^+\approx 50$ and $r_z^+\approx 75$ for Newtonian fluid and the Oldroyd-B model, respectively. It is well known in wall-bounded turbulent flow that the averaged streak spacing λ_z^+ corresponds to twice the length of r_z^+ in which the two-point correlation coefficient of streamwise velocity fluctuation R_{uu} is minimum.[56] Therefore, the averaged streak spacing is $\lambda_z^+\approx 100$ for Newtonian fluid and $\lambda_z^+\approx 150$ for the Oldroyd-B model; i.e., the streak spacing for the Oldroyd-B model is about 1.5 times larger than that for Newtonian fluid at $y/\theta_0=0.152$ and $x/\theta_0=100.8$. On the other hand, the difference in the streak spacing between the Giesekus model and Newtonian fluid is very small. Here, it has been reported in the drag-reducing turbulent channel flow that the streak spacing becomes larger with the increase in drag reduction. This is consistent with the present result in which the streak spacing for the Oldroyd-B model with the larger drag reduction ratio is larger than that for the Giesekus model with the smaller drag reduction ratio.

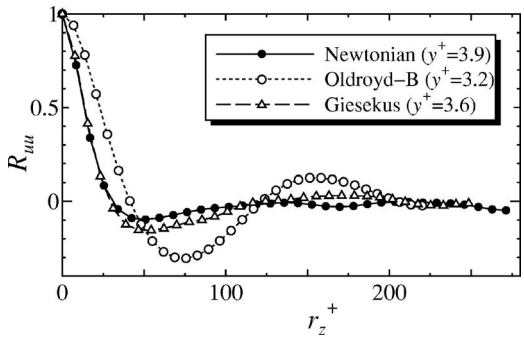

FIG. 20. Two-point correlation coefficient of streamwise velocity fluctuation at $y/\theta_0=0.152$ and $x/\theta_0=100.8$.

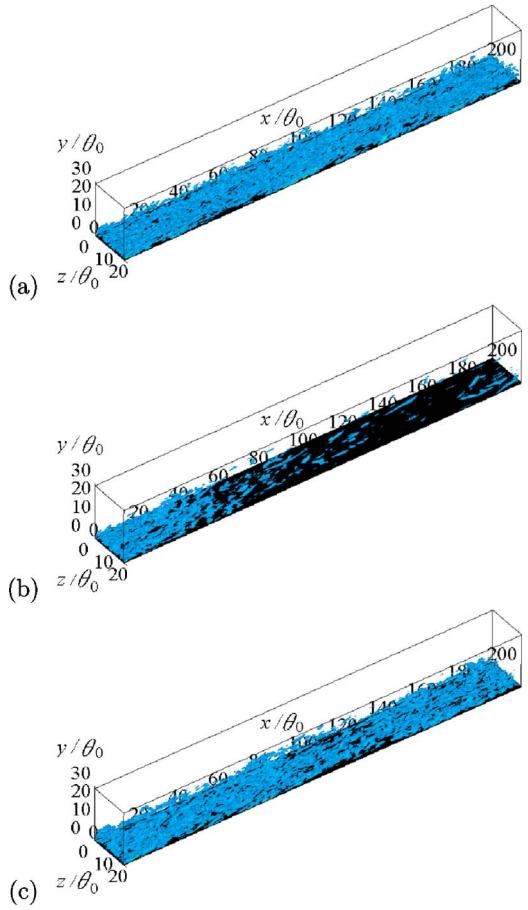

FIG. 21. (Color online) Isosurface of second invariant of velocity gradient tensor ($Q\theta_0^2/U_e^2=0.005$, blue). Flow is from left to right: (a) Newtonian fluid, (b) Oldroyd-B model, and (c) Giesekus model.

Next, the isosurface of the second invariant of the velocity gradient tensor $Q\theta_0^2/U_e^2=0.005$ is shown in Fig. 21. The region in which the second invariant $Q=-(\partial u_i/\partial x_j)\times(\partial u_j/\partial x_i)/2$ is positive represents the region in which the strength of rotation overcomes the strain rate, and corresponds to the region where the vortices exist.[60] In the figure, the flow is from left to right, and the black area represents the wall. For Newtonian fluid, there are numerous quasi-streamwise vortices near the wall in the region from the inlet to outlet. For the Oldroyd-B model, for $x/\theta_0>50$, only a few quasi-streamwise vortices can be seen. For the Giesekus model, the quasi-streamwise vortices are slightly different from that for Newtonian fluid in the center region ($90<x/\theta_0<130$). Note that the region of the vortices depends

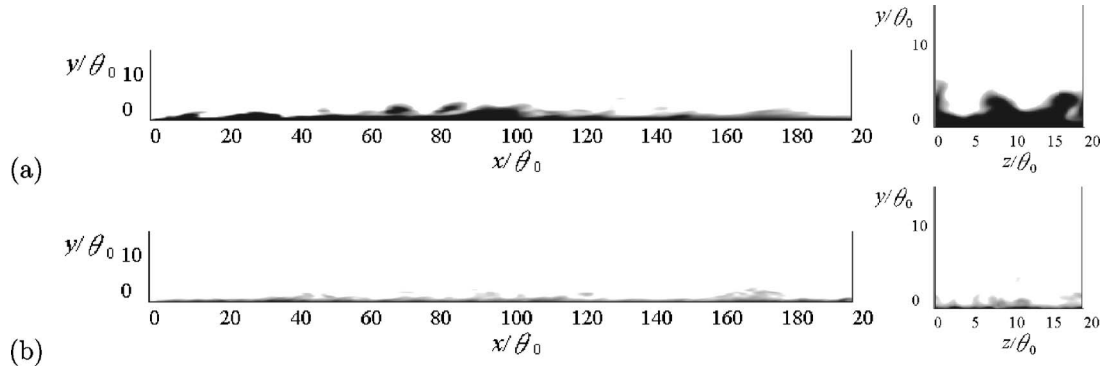

FIG. 22. Contour of elastic energy ($0 \leqslant k_p \leqslant 0.0025$, white to black) in the x-y plane at $z/\theta_0=0$ and the y-z plane at $x/\theta_0=100.8$: (a) Oldroyd-B model, (b) Giesekus model.

somewhat on the Q criterion and the time. As shown in Fig. 11, the trace of mean viscoelastic stress $\overline{E_{kk}}^+$ for the Oldroyd-B model is larger than that for the Giesekus model in the region $1 \leqslant y^+ \leqslant 50$. Therefore, we can assume that near-wall coherent structures are strongly affected by the high elongational viscosity, and the effect appears significantly for $x/\theta_0 > 50$, in which the quasi-streamwise vortices are weakened and become larger in the streamwise direction, compared to Newtonian fluid.

To investigate the transport of the elastic energy,[35,36] $k_p=(1-\beta)E_{kk}/(2\mathrm{Re}_{\theta_0})$, near the wall, the contour of elastic energy in the x-y plane at $z/\theta_0=0$ and the y-z plane at $x/\theta_0=100.8$ are shown in Fig. 22. For the Giesekus model with the smaller drag reduction ratio, large elastic energy exists only in the region very close to the wall, while for the Oldroyd-B model with the larger drag reduction ratio, large elastic energy near the wall is transported to near the center of the turbulent boundary layer ($y/\theta_0 \simeq 5$). This corresponds to the fact that the trace of mean viscoelastic stress $\overline{E_{kk}}^+$ for the Oldroyd-B model is large in the region away from the wall ($y^+ \simeq 100$), while $\overline{E_{kk}}^+$ for the Giesekus model suddenly decreases away from the wall (see Fig. 11). In addition, the present result is consistent with the finding of Min *et al.*[35,36] for the drag-reducing turbulent channel flow in which without drag reduction, high elastic energy exists only very near the wall, while with drag reduction (%DR=20), this energy very near the wall is transported to the buffer and log layers.

Min *et al.*[35,36] claimed that the extensional viscosity effect alone made it difficult to explain the onset of the drag reduction and presented the following scenario for the mechanism of drag reduction based on the elastic energy. When the drag reduction occurs, the turbulent kinetic energy near the wall is absorbed by the polymer and transformed into elastic energy. This elastic energy is lifted up by the near-wall vortex motion and released as turbulent kinetic energy or is dissipated in the buffer and log layers. In the present study, the distinct difference in turbulence statistics near the wall between the drag-reducing and Newtonian fluids is observed, as reported in the drag-reducing turbulent channel flow. Therefore, it can be deduced that the drag-reducing mechanism in the present study is similar to that presented by Min *et al.*[35–37] for the turbulent channel flow. In the outer region, distributions of turbulence statistics for the drag-reducing fluid are similar to those for Newtonian fluid. This indicates that the elastic energy does not reach the outer region of the turbulent boundary layer for both the Oldroyd-B and Giesekus models (see Fig. 22). Note that for the drag-reducing turbulent channel flow,[35–37] turbulence statistics are different even at the center of the channel. Another drag-reducing mechanism was proposed by Dubief *et al.*,[29,32] who used the modified autoregeneration cycle of near-wall turbulence, taking into account the action of polymers on turbulent structures. Their drag-reducing mechanism derives from the study of small-scale quantities such as polymer work. For examination of the drag-reducing mechanism proposed by Dubief *et al.*[29,32] for the turbulent boundary layer flow, further investigation of the correlation between velocity and polymer body force would be needed.

Figure 23 shows the velocity vector in the y-z plane and contour of the second invariant of velocity gradient tensor Q at $x/\theta_0=100.8$ for Newtonian fluid and the Oldroyd-B model. In the figure, the abscissa and ordinate are spanwise

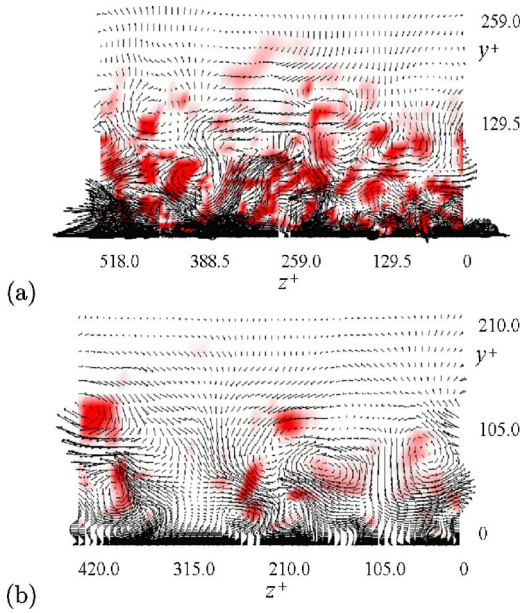

FIG. 23. (Color online) Velocity vector in the y-z plane and contour of Q ($0 \leqslant Q\theta_0^2/U_e^2 \leqslant 0.005$, white to red) at $x/\theta_0=100.8$: (a) Newtonian fluid, (b) Oldroyd-B model.

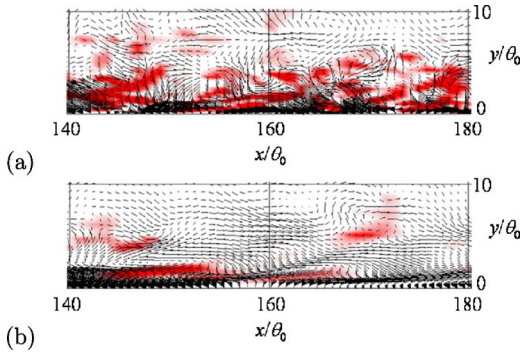

FIG. 24. (Color online) Velocity vector in the x-y plane and contour of Q ($0 \leqslant Q\theta_0^2/U_e^2 \leqslant 0.005$, white to red) at $z/\theta_0=5.563$: (a) Newtonian fluid, (b) Oldroyd-B model.

and wall-normal wall units z^+ and y^+, respectively. For the Oldroyd-B model, the quasi-streamwise vortices are hardly observed, unlike the Newtonian fluid, and a few quasi-streamwise vortices exist in the region relatively away from the wall.

To investigate the streamwise variation of the near-wall coherent structures, the velocity vector in the x-y plane and contour of the second invariant Q at $z/\theta_0=5.563$ are shown in Fig. 24. Owing to the streamwise development of the turbulent boundary layer, one must first obtain the time-averaged velocity at all the streamwise locations within the computational domain, and then evaluate the velocity fluctuation in the y-z plane from the time-averaged velocity. However, the implementation of such a procedure is quite expensive. Therefore, in the present study, turbulence statistics in the y-z plane at all the streamwise locations are estimated by interpolating ones at 20 different streamwise locations, and then the velocity fluctuations in the y-z plane are obtained at all the streamwise locations for saving the computational cost. For Newtonian fluid, some fine near-wall vortices can be observed, whereas with the Oldroyd-B model, a near-wall vortex enlarged in the streamwise direction is observed in the region $140 \leqslant x/\theta_0 \leqslant 170$.

V. CONCLUSIONS

Direct numerical simulation of a zero-pressure gradient drag-reducing turbulent boundary layer of homogeneous viscoelastic fluids was performed at momentum-thickness Reynolds number $\mathrm{Re}_{\theta_0}=500$ and Weissenberg number $\mathrm{We}=25$ using constitutive equation models such as the Oldroyd-B and Giesekus models.

The maximum drag reduction ratio for the Oldroyd-B model (%DR=42), which has the higher elongational viscosity, is larger than that for the Giesekus model (%DR=16) under the present numerical conditions. A distinct difference is observed in turbulence statistics such as turbulence intensities and Reynolds shear stress near the wall between the Oldroyd-B model and Newtonian fluid, as reported in the drag-reducing turbulent channel flow. In the outer region, on the other hand, distributions of turbulence statistics for the Oldroyd-B model with a drag reduction ratio of about 40% are similar to those for Newtonian fluid, which is consistent with the experiment of the drag-reducing turbulent boundary layer of surfactant solutions but different from that of the drag-reducing turbulent channel flow where turbulence statistics are smaller across the channel. The relation in magnitude of maximum values of streamwise turbulence intensity between the Oldroyd-B model and Newtonian fluid varies in the streamwise direction. This indicates that the maximum value of streamwise turbulence intensity for the turbulent boundary layer does not seem to be directly related to the amount of the drag reduction. The modification of the streamwise and wall-normal turbulence intensities near the wall can be explained by investigating the profiles of pressure-strain correlation terms and the anisotropy invariant map for Reynolds stress tensor, following the previous study on the drag-reducing turbulent channel flow.

To investigate the drag-reducing mechanism for the turbulent boundary layer, budgets of turbulent kinetic energy and Reynolds normal stresses, which have not been reported for the drag-reducing turbulent boundary layer, were investigated. According to the streamwise variation in the relation between the production term and drag reduction ratio, it is deduced that the production term for the turbulent boundary layer does not correspond to the amount of drag reduction, which is consistent with the fact that the streamwise turbulence intensity profile is not a direct indication of drag reduction. Compared to the Giesekus model, the contribution of the polymer stress work to the turbulent kinetic energy budget for the Oldroyd-B model with the larger drag reduction ratio is larger, whose trend is the same as the drag-reducing turbulent channel flow. The contribution of the advection term to the budget of streamwise Reynolds normal stress, which does not appear for the turbulent channel flow, is not negligible near the wall for the Oldroyd-B model.

For the Oldroyd-B model with the maximum drag reduction ratio of 42%, for $x/\theta_0 > 50$, the low-speed region is considerably larger than that for Newtonian fluid, and the quasi-streamwise vortices are weakened and become larger in the streamwise direction, compared to Newtonian fluid. On the other hand, near-wall coherent structures such as near-wall streak structures and quasi-streamwise vortices for the Giesekus model with the maximum drag reduction ratio of 16% are slightly larger than those for Newtonian fluid. The difference in modification of near-wall coherent structures between the Oldroyd-B and Giesekus models can be explained by using the trace of mean viscoelastic stress and the elastic energy presented by Min *et al.*[36] for the drag-reducing turbulent channel flow, which represent the elongational viscosity effect. Hence, we can deduce that the higher extensional viscosity is the key to yield higher drag reduction and the larger modification of turbulence statistics and coherent structures for the turbulent boundary layer, and the drag-reducing mechanism is essentially the same as that for the drag-reducing turbulent channel flow, at least in the inner region.

Unfortunately, the agreement of mean velocity and turbulence statistics between the present DNS and the previous experiments is not satisfactory. This is because the inlet boundary condition, the Reynolds number, and the amount of drag reduction for the present numerical simulation are dif-

ferent from those for the experiments. In addition, we used the Oldroyd-B and Giesekus models, which were simple rheological models, for the fixed mobility factor and the viscosity ratio, in order to investigate the effect of elasticity easily. For better comparison between the DNS and experiments, further DNS is warranted under the numerical conditions corresponding to the existing experiments.

ACKNOWLEDGMENTS

We are grateful to Professor Y. Morinishi of Nagoya Institute of Technology and Professor Y. Kawaguchi of the Tokyo University of Science for their valuable suggestions on constructing the present DNS code. Special thanks are also due to S. Hotta for the assistance with the numerical simulations.

[1] T. S. Luchik and W. G. Tiederman, "Turbulent structure in low-concentration drag-reducing channel flows," J. Fluid Mech. **190**, 241 (1988).
[2] D. T. Walker and W. G. Tiederman, "Turbulent structure in a channel flow with polymer injection at the wall," J. Fluid Mech. **218**, 377 (1990).
[3] F. T. Pinho and J. H. Whitelaw, "Flow of non-Newtonian fluids in a pipe," J. Non-Newtonian Fluid Mech. **34**, 129 (1990).
[4] K. J. Harder and W. G. Tiederman, "Drag reduction and turbulent structure in two-dimensional channel flows," Philos. Trans. R. Soc. London, Ser. A **336**, 19 (1991).
[5] T. Wei and W. W. Willmarth, "Modifying turbulent structure with drag-reducing polymer additives in turbulent channel flows," J. Fluid Mech. **245**, 619 (1992).
[6] A. Gyr and H.-W. Bewersdorff, *Drag Reduction of Turbulent Flows by Additives* (Kluwer Academic, Dordrecht, The Netherlands, 1995).
[7] J. M. J. Den Toonder, M. A. Hulsen, G. D. C. Kuiken, and F. T. M. Nieuwstadt, "Drag reduction by polymer additives in a turbulent pipe flow: Numerical and laboratory experiments," J. Fluid Mech. **337**, 193 (1997).
[8] M. Itoh, S. Imao, and K. Sugiyama, "Characteristics of low-speed streaks in the flow of drag-reducing surfactant solution," JSME Int. J., Ser. B **40**, 550 (1997).
[9] M. D. Warholic, H. Massah, and T. J. Hanratty, "Influence of drag-reducing polymers on turbulence: Effects of Reynolds number, concentration and mixing," Exp. Fluids **27**, 461 (1999).
[10] M. D. Warholic, G. M. Schmidt, and T. J. Hanratty, "The influence of a drag-reducing surfactant on a turbulent velocity field," J. Fluid Mech. **388**, 1 (1999).
[11] M. D. Warholic, D. K. Heist, M. Katcher, and T. J. Hanratty, "A study with particle-image velocimetry of the influence of drag-reducing polymers on the structure of turbulence," Exp. Fluids **31**, 474 (2001).
[12] P. K. Ptasinski, F. T. M. Nieuwstadt, B. H. A. A. Van den Brule, and M. A. Hulsen, "Experiments in turbulent pipe flow with polymer additives at maximum drag reduction," Flow, Turbul. Combust. **66**, 159 (2001).
[13] Y. Kawaguchi, T. Segawa, Z. Feng, and P. Li, "Experimental study on drag-reducing channel flow with surfactant additives—Spatial structure of turbulence investigated by PIV system," Int. J. Heat Fluid Flow **23**, 700 (2002).
[14] F.-C. Li, Y. Kawaguchi, T. Segawa, and K. Hishida, "Reynolds-number dependence of turbulence structures in a drag-reducing surfactant solution channel flow investigated by particle image velocimetry," Phys. Fluids **17**, 075104 (2005).
[15] F.-C. Li, Y. Kawaguchi, K. Hishida, and M. Oshima, "Investigation of turbulence structures in a drag-reduced turbulent channel flow with surfactant additive by stereoscopic particle image velocimetry," Exp. Fluids **40**, 218 (2006).
[16] J. Koskie and W. G. Tiederman, "Polymer drag reduction of a zero-pressure-gradient boundary layer," Phys. Fluids A **3**, 2471 (1991).
[17] H. L. Fontaine, H. Petrie, and T. A. Brungart, "Velocity profile statistics in a turbulent boundary layer with slot-injected polymer," J. Fluid Mech. **238**, 435 (1992).
[18] C. M. White, V. S. R. Somandepalli, and M. G. Mungal, "The turbulence structure of drag-reduced boundary layer flow," Exp. Fluids **36**, 62 (2004).
[19] Y. Hou, V. S. R. Somandepalli, and M. G. Mungal, "A technique to determine total shear stress and polymer stress profiles in drag reduced boundary layer flows," Exp. Fluids **40**, 589 (2006).
[20] M. Itoh, S. Tamano, K. Yokota, and M. Ninagawa, "Velocity measurement in turbulent boundary layer of drag-reducing surfactant solution," Phys. Fluids **17**, 075107 (2005).
[21] R. Sureshkumar, A. N. Beris, and R. A. Handler, "Direct numerical simulation of the turbulent channel flow of a polymer solution," Phys. Fluids **9**, 743 (1997).
[22] C. D. Dimitropoulos, R. Sureshkumar, and A. N. Beris, "Direct numerical simulation of viscoelastic turbulent channel flow exhibiting drag reduction: Effect of the variation of rheological parameters," J. Non-Newtonian Fluid Mech. **79**, 433 (1998).
[23] C. D. Dimitropoulos, R. Sureshkumar, A. N. Beris, and R. A. Handler, "Budgets of Reynolds stress, kinetic energy and streamwise enstrophy in viscoelastic turbulent channel flow," Phys. Fluids **13**, 1016 (2001).
[24] S. Sibilla and A. Baron, "Polymer stress statistics in the near-wall turbulent flow of a drag-reducing solution," Phys. Fluids **14**, 1123 (2002).
[25] E. De Angelis, C. M. Casciola, and R. Piva, "DNS of wall turbulence: Dilute polymers and self-sustaining mechanisms," Comput. Fluids **31**, 495 (2002).
[26] P. K. Ptasinski, B. J. Boersma, F. T. M. Nieuwstadt, M. A. Hulsen, B. H. A. A. Van den Brule, and J. C. R. Hunt, "Turbulent channel flow near maximum drag reduction: Simulations, experiments and mechanisms," J. Fluid Mech. **490**, 251 (2003).
[27] Q. Zhou and R. Akhavan, "A comparison of FENE and FENE-P dumbbell and chain models in turbulent flow," J. Non-Newtonian Fluid Mech. **109**, 115 (2003).
[28] K. D. Housiadas and A. N. Beris, "Polymer-induced drag reduction: Effects of the variations in elasticity and inertia in turbulent viscoelastic channel flow," Phys. Fluids **15**, 2369 (2003).
[29] Y. Dubief, C. M. White, V. E. Terrapon, E. S. G. Shaqfeh, P. Moin, and S. K. Lele, "On the coherent drag-reducing and turbulence-enhancing behaviour of polymers in wall flows," J. Fluid Mech. **514**, 271 (2004).
[30] K. D. Housiadas and A. N. Beris, "An efficient fully implicit spectral scheme for DNS of turbulent viscoelastic channel flow," J. Non-Newtonian Fluid Mech. **122**, 243 (2004).
[31] K. D. Housiadas, A. N. Beris, and R. A. Handler, "Viscoelastic effects on higher order statistics and on coherent structures in turbulent channel flow," Phys. Fluids **17**, 035106 (2005).
[32] Y. Dubief, V. Terrapon, C. M. White, E. G. Shaqreh, P. Moin, and S. K. Lele, "New answers on the interaction between polymers and vortices in turbulent flows," Flow, Turbul. Combust. **74**, 311 (2005).
[33] C.-F. Li, V. K. Gupta, R. Sureshkumar, and B. Khomami, "Turbulent channel flow of dilute polymeric solutions: Drag reduction scaling and an eddy viscosity model," J. Non-Newtonian Fluid Mech. **139**, 177 (2006).
[34] C.-F. Li, R. Sureshkumar, and B. Khomami, "Influence of rheological parameters on polymer induced turbulent drag reduction," J. Non-Newtonian Fluid Mech. **140**, 23 (2006).
[35] T. Min, J. Y. Yoo, H. Choi, and D. D. Joseph, "A role of elastic energy in turbulent drag reduction by polymer additives," Proceedings of the 2nd Turbulence and Shear Flow Phenomena, Stockholm, Sweden (2001), Vol. 1, pp. 35–40.
[36] T. Min, J. Y. Yoo, H. Choi, and D. D. Joseph, "Drag reduction by polymer additives in a turbulent channel flow," J. Fluid Mech. **486**, 213 (2003).
[37] T. Min, H. Choi, and J. Y. Yoo, "Maximum drag reduction in a turbulent channel flow by polymer additives," J. Fluid Mech. **492**, 91 (2003).
[38] B. Yu and Y. Kawaguchi, "Effect of Weissenberg number on the flow structure: DNS study of drag-reducing flow with surfactant additives," Int. J. Heat Fluid Flow **24**, 491 (2003).
[39] B. Yu and Y. Kawaguchi, "Direct numerical simulation of viscoelastic drag-reducing flow: A faithful finite difference method," J. Non-Newtonian Fluid Mech. **116**, 431 (2004).
[40] B. Yu, F. Li, and Y. Kawaguchi, "Numerical and experimental investigation of turbulent characteristics in a drag-reducing flow with surfactant additives," Int. J. Heat Fluid Flow **25**, 961 (2004).
[41] B. Yu and Y. Kawaguchi, "Parametric study of surfactant-induced drag-reduction by DNS," Int. J. Heat Fluid Flow **27**, 887 (2006).
[42] C. D. Dimitropoulos, Y. Dubief, E. S. G. Shaqfeh, P. Moin, and S. K. Lele, "Direct numerical simulation of polymer-induced drag reduction in turbulent boundary layer flow," Phys. Fluids **17**, 011702 (2005).

[43]M. Shin and E. S. G. Shaqfeh, "Viscoelastic turbulent boundary layer with near-wall injection of polymer molecules," *Annual Research Briefs 2005, Center for Turbulence Research* (NASA Ames/Stanford University, Stanford, 2005), pp. 389–405.
[44]C. D. Dimitropoulos, Y. Dubief, E. S. G. Shaqfeh, and P. Moin, "Direct numerical simulation of polymer-induced drag reduction in turbulent boundary layer flow of inhomogeneous polymer solutions," J. Fluid Mech. **566**, 153 (2006).
[45]R. B. Bird, R. C. Armstrong, and O. Hassager, *Dynamics of Polymeric Liquids. Volume 1: Fluid Mechanics*, 2nd ed. (Wiley Interscience, New York, 1987).
[46]T. S. Lund, X. Wu, and K. D. Squires, "Generation of turbulent inflow data for spatially-developing boundary layer simulations," J. Comput. Phys. **140**, 233 (1998).
[47]J. K. Dukowicz and A. S. Dvinsky, "Approximate factorization as a high order splitting for the implicit incompressible flow equations," J. Comput. Phys. **102**, 336 (1992).
[48]R. Sureshkumar and A. N. Beris, "Effect of artificial stress diffusivity on the stability of numerical calculations and the flow dynamics of time-dependent viscoelastic flows," J. Non-Newtonian Fluid Mech. **60**, 53 (1995).
[49]P. R. Spalart, "Direct simulation of a turbulent boundary layer up to $\mathrm{Re}_\theta = 1410$," J. Fluid Mech. **187**, 61 (1988).
[50]D. E. Coles, "The turbulent boundary layer in a compressible fluid," Report No. R-403-PR, The Rand Corp., Santa Monica, CA (1962).
[51]M. Tabor and P. G. De Gennes, "A cascade theory of drag reduction," Europhys. Lett. **2**, 519 (1986).
[52]J. L. Lumley, "Drag reduction by additives," Annu. Rev. Fluid Mech. **1**, 367 (1969).
[53]J. L. Lumley, "Drag reduction in turbulent flow by polymer additives," J. Polym. Sci. Macromol. Rev. **7**, 263 (1973).
[54]P. Orlandi, "A tentative approach to the direct simulation of drag reduction by polymers," J. Non-Newtonian Fluid Mech. **60**, 277 (1995).
[55]P. S. Virk, "Drag reduction fundamentals," AIChE J. **21**, 625 (1975).
[56]J. Kim, P. Moin, and R. Moser, "Turbulence statistics in fully developed channel flow at low Reynolds number," J. Fluid Mech. **177**, 133 (1987).
[57]J. L. Lumley and G. R. Newman, "The return to isotropy of homogeneous turbulence," J. Fluid Mech. **82**, 161 (1977).
[58]J. Jovanović, M. Pashtrapanska, B. Frohnapfel, F. Durst, J. Koskinen, and K. Koskinen, "On the mechanism responsible for turbulent drag reduction by dilute addition of high polymers: Theory, experiments, simulations, and predictions," J. Fluids Eng. **128**, 118 (2006).
[59]B. Frohnapfel, P. Lammers, J. Jovanović, and F. Durst, "Interpretation of the mechanism associated with turbulent drag reduction in terms of anisotropy invariants," J. Fluid Mech. **577**, 457 (2007).
[60]Y. Dubief and F. Delcayre, "On coherent-vortex identification in turbulence," J. Turbul. **1**, 1 (2000).